Energy, Mines and Resources Canada
Énergie, Mines et Ressources Canada

CANMET
Canada Centre for Mineral and Energy Technology
Centre canadien de la technologie des minéraux et de l'énergie

PREPARATION OF A CERAMIC ELECTROLYTE IN THE SYSTEM $MgO-K_2O-TiO_2$

H.H. Quon and T.A.Wheat

AUGUST 1977

ENERGY RESEARCH PROGRAM
MINERAL SCIENCES LABORATORIES
CANMET REPORT 78-8

Available by mail from:

Printing and Publishing
Supply and Services Canada,
Ottawa, Canada K1A 0S9

CANMET
Energy, Mines and Resources Canada,
555 Booth St.,
Ottawa, Canada K1A 0G1

or through your bookseller.

Catalogue No. M38–13/78-8 Price: Canada: $3.00
ISBN 0-660-10006-1 Other countries: $3.60

Price subject to change without notice.

En vente par la poste:

Imprimerie et Édition
Approvisionnements et Services Canada,
Ottawa, Canada K1A 0S9

CANMET
Énergie, Mines et Ressources Canada,
555, rue Booth
Ottawa, Canada K1A 0G1

ou chez votre libraire.

Nº de catalogue M38–13/78-8 Prix: Canada: $3.00
ISBN 0-660-10006-1 Autres pays: $3.60

Prix sujet à changement sans avis préalable.

PREPARATION OF A CERAMIC ELECTROLYTE IN THE SYSTEM $MgO-K_2O-TiO_2$

by

D.H.H. Quon* and T.A. Wheat*

- - -

ABSTRACT

The present work forms part of a program to develop ionically conducting materials for potential use in energy conversion systems. Having applications in high energy-density batteries, fuel cells and sensors, these materials are playing an increasingly important role in the development of much more efficient energy storage and conversion devices.

Of the over 30 known solid-state ionically conducting materials, those having compositions in the $MgO-K_2O-TiO_2$ system have been reported to possess electrical properties that are borderline to those required for battery applications. However, the very limited data available in the literature has all been obtained using poor quality, inhomogeneous material produced from ball milled materials. Consequently, it is of great importance to determine the intrinsic properties of this potentially significant group of materials. For this purpose, a wet process has been developed to produce the needed homogeneous, high quality sintered compositions.

For comparative purposes, materials having the composition $K_xMg_{x/2}Ti_{8-x/2}O_{16}$ where $1.4 \leq x \leq 2.0$ were prepared using both a conventional ball milling technique and a novel wet chemical process. It is shown that the latter method produces homogeneous material that can readily be sintered close to the theoretical density, whereas the former method produces inhomogeneous material that can only be sintered to approximately 90% theoretical density.

Using the reactive, homogeneous, chemically prepared materials, it has been established that two-phase systems are developed when x equals 1.4 and 2.0. At high titania concentrations where x equals 1.4, rutile is formed, whereas at low titania concentrations where x equals 2.0, a new phase is formed which is isostructural with $K_yLi_yTi_{4-y/2}O_8$. At intermediate compositions where $1.5 \leq x \leq 1.8$, single-phase material is formed.

---

*Research Scientist, Ceramic Section, Industrial Minerals Laboratory, Mineral Sciences Laboratories, Canada Centre for Mineral and Energy Technology, Department of Energy, Mines and Resources, Ottawa, Canada.

LA PREPARATION D'UN ELECTROLYTE CERAMIQUE DANS LE SYSTEME $MgO-K_2O-TiO_2$

par

H.H. Quon* et T.A. Wheat*

RESUME

La présente recherche fait partie d'un programme de mise au point de conducteurs ioniques susceptibles d'être employés dans les systèmes de transformation de l'énergie. Ces matériaux jouent un rôle de plus en plus important lors de la mise au point de dispositifs plus efficaces d'emmagasinage et de transformation de l'énergie tels que les piles énergétiques à haute densité, les piles et les détecteurs à combustible.

Plus de 30 conducteurs ioniques à l'état solide sont connus. On reporte que ceux ayant la composition du système $MgO-K_2O-TiO_2$ possèdent des propriétes électriques se rapprochant de celles recherchées pour l'usage dans les piles. Le nombre limité de données disponibles jusqu'à présent a été obtenu à partir de matériau de pauvre qualité non-homogène provenant de matériaux broyés. En conséquence, il est important de pouvoir déterminer les propriétés intrinsèques de ce groupe de matériaux ayant une portée éventuelle. A cette fin, un procédé par voie humide a été mis au point afin de produire les compositions frittées, homogènes et de haute qualité voulues.

A des fins comparatives, les matériaux ayant la composition $K_xMg_{x/2}Ti_{8-x/2}O_{16}$ où $1.4 \leqslant x \leqslant 2.0$ ont été préparés selon la technique classique du broyeur à boulet et selon le nouveau procédé chimique par voie humide. La dernière méthode donne un matériau homogène susceptible d'être fritté près de la densité théorique tandis que la première donne un matériau non-homogène ne pouvant être fritté qu'à environ 90% de la densité théorique.

Lorsqu'on emploie les matériaux réactifs, homogènes et préparés chimiquement, il a été établi que les systèmes biphasés sont mis au point lorsque x est égal à 1.4 et 2.0. Lorsque la concentration du titane est élevé, x égale 1.4, le rutile est formé; mais si la concentration du titane est faible, x égale 2.0, une nouvelle phase isostructurale avec le $K_yLi_yTi_{4-y/2}O_8$ est formée. Les compositions intermédiaires $1.5 \leqslant x \leqslant 1.8$ provoquent la formation d'un matériau à une seule phase.

*Chercheur scientifique, Section de la céramique, Laboratoire des minéraux industriels, Laboratoires des sciences minérales, Centre canadien de la technologie des minéraux et de l'énergie, Ministère de l'Energie, des Mines et des Ressources, Ottawa, Canada.

CONTENTS

FIGURES

TABLES

INTRODUCTION

Interest in the occurrence and application of solid-state ceramic electrolytes was stimulated by the pioneering work of Kiukkola and Wagner in 1957 who demonstrated that calcia-doped zirconia could be used satisfactorily in an electrochemical cell to determine the thermodynamic stability of various compounds and alloys at elevated temperatures[1]. The authors also showed that the ac conductivity of this electrolyte was essentially independent of oxygen partial pressure in the range between 1 and 1×10^{-20} atm (1×10^{5} to 1×10^{-15} Pa) indicating that the electronic conductivity played only a minor role in the overall conductivity. With recognition that this very refractory material (mp $\sim$2700°C) could be used as an electrolyte, a considerable effort has been expended over the last twenty years to exploit these properties and also to seek other materials that might behave in a similar fashion.

At present, over thirty ceramic materials are known to be ionically conductive[2]. Some of the more important include both anionic and cationic conductors. Perhaps the most prominent examples of each family are the electrolytes: doped zirconia and beta-alumina. The anionically conducting zirconias have been exploited in the development of oxygen concentration cells such as oxygen-hydrogen fuel cells and in fabrication of oxygen probes for use in gases or liquid metals[3,4,5]. Similarly, cationically conducting beta-alumina is presently under development to produce the electrolyte for a new

generation of secondary storage batteries having an energy density approximately nine times that of a conventional Pb-acid cell[6,7]. This electrolyte has also been used as the active element in sodium probes in nuclear reactors and metal fining operations. The characteristics of these and other ceramic electrolytes have recently been reviewed by Worrell who notes that a number of other anionic conductors are known, such as BaC_2 dissolved in BaF_2 (carbon conducting), Y_2S_3 dissolved in CaS (sulphur conducting) and AlN (nitrogen conducting)[8]. The commercial applications of electrolytes such as these are very wide. For example, each would be useable in a concentration cell for accurate and rapid determination of the concentration of these elements in a process. Alternatively, they could conceivably be used in purification processes in which the element concerned could be selectively removed from or added to a gas or liquid. A study to examine the electrolytic deoxidation of steel using a zirconia-based material has been underway in Ohio State University for several years[9].

Although the examples given above are only applicable to above ambient temperatures, a number of these newer solid-state electrolytes are extremely good ionic conductors at room temperature. Among this group are the silver rubidium iodides ($RbAg_4I_5$) and the silver iodophosphates ($Ag_{19}I_{15}P_2O_7$). These silver-conducting materials have been used in a variety of timers, coulometers and batteries[10]. At present a small solid-state coulometer the size of a button is manufactured for use in

electrical equipment to monitor usage[11].

Because of these important applications and their potential for energy-related economies to be made either through equipment control such as monitoring flue gases or automobile exhausts to optimize combustion, or through process control such as the fining of liquid copper or steel and other metals, there is a continuing interest in electrolytes as a whole. Because of their application, particularly in probes and batteries, it is desirable to have the ionic conductivity as high as possible and the electronic conductivity as low as possible. Unfortunately, these properties are particularly sensitive to low concentrations of impurities and much of the earlier work, including that of Kiukkola and Wagner[1], was conducted with electrolytes that were synthesized from contaminated raw materials or that became contaminated during processing, e.g., through the use of a ball mill stage in preparing the raw material. Consequently, it is most desirable to examine the physical and chemical characteristics of electrolytes using high-quality material, so that the properties under examination are intrinsic rather than extrinsic to that material.

Although the mineral hollandite and structurally related minerals have been known for some time, it was only recently recognized that materials having a hollandite structure were effective cationic conductors. These materials crystallize in the tetragonal system and form tunnels in the c-direction through which group I or group II cations may move under an applied chemical or electrical potential. Little is known of the

characteristics of the material $K_xMg_{x/2}Ti_{8-x/2}O_{16}$. Takahashi and Kuwabara describe preliminary data obtained on a series of materials in which x varied from 1.4 to 2.0[12]. Unfortunately, their materials were prepared by ball milling oxides or carbonates followed by a calcination stage, forming, and subsequent firing. Under these conditions, inhomogeneous, very coarse-grained specimens were produced. Similarly, Roth et al. describe the lithium analogue prepared by the same process[13].

Because of their inhomogeneity the materials would be unsuitable for electrolytic applications and the large crystal size will tend to give mechanically weaker material. In addition, because of the relatively unreactive nature of ball milled materials, high firing temperatures, and relatively long sintering times are required both of which lead to a selective loss of potassium and the development of a macro-inhomogeneity. Consequently, a series of experiments were conducted to prepare and characterize different potassium-doped magnesium titanates that had been developed using homogeneous chemically prepared raw materials. Although unsuitable for extensive examination, a series of compositions was also prepared using a ball milling process. The object of this initial stage was to develop a series of crude materials that could be used to obtain basic X-ray powder diffraction patterns while the rather time-consuming procedure of preparing the high quality raw materials was underway.

EXPERIMENTAL PROCEDURE

Materials in the $MgO-K_2O-TiO_2$ systems were compounded by each of two methods so that the final fired composition corresponded to the formula: $K_xMg_{x/2}Ti_{8-x/2}O_{16}$ where x was between 1.4 and 2.0. In each case, the mixed raw materials were initially calcined to develop crystalline phases prior to milling, forming, and finally firing to produce high-density bodies. However, the methods to produce the initial raw material compositions were quite different. As noted, a conventional ball milling procedure was used to prepare the initial samples for reference purposes. For purposes of the actual investigation, in anticipation of unacceptable inhomogeneity being retained in the ball milled materials, a series of wet chemically prepared compositions was also examined.

I. Conventionally Ball Milled Raw Materials

Appropriate quantities of MgO (certified A.C.S. grade, Fisher Scientific Co., Fairlawn, N.J.), K_2CO_3, and TiO_2 (reagent grade, Anachemia Chemicals Ltd., Toronto) reagents were initially hand mixed using an agate pestle and mortar and subsequently mixed in a polyethylene container in a Turbula mixer for 1 hr. The various compositions were subsequently calcined in air at 1100°C for 1 hr; in each case the material was placed in a Pt-lined ZrO_2 boat. The calcined materials were then ball milled in a high-alumina mill using 1.27-cm (0.5-in.) diameter high-alumina cylinders for 2 hr. Samples of each composition were mixed with 5% polyvinyl alcohol using a 10% solution of PVA

in water and formed by uniaxially pressing in a steel die assembly under a pressure of 70 MPa (10,000 psi) to produce discs 2.5 cm in diameter and 5 mm in height. The discs were finally sintered in air at either 1180°C for 4 hr or at 1200°C for 15 hr; in all cases the materials were contained in a Pt-lined ZrO_2 boat. Sintering was conducted using an electrically heated Globar furnace that operated to produce the heating schedule given in Figure 1. On completion of sintering, the samples were allowed to cool naturally within the furnace.

II. Wet Chemically Prepared Raw Materials

To ensure homogeneity in the samples, it was clear that some form of wet chemical processing would be necessary. In general, the methods available for producing homogeneous ceramic powders involve the formation of a solution of the reagents or their precursors, followed by either co-precipitation, gelation or flash-drying. The co-precipitation technique has been used for some time on an industrial scale to produce homogeneous finely divided raw materials for piezoelectric applications. However, close control must be maintained to prevent significant segregation due to widely differing precipitation rates. The same difficulty can arise with a sol-gel process to produce the raw materials, particularly if the dopant salts are nitrates. It is for this reason that an adaptation of the flash-drying process was used in the present work.

Ideally, the most appropriate process to form homogeneous raw materials would be to prepare the appropriate clear solution

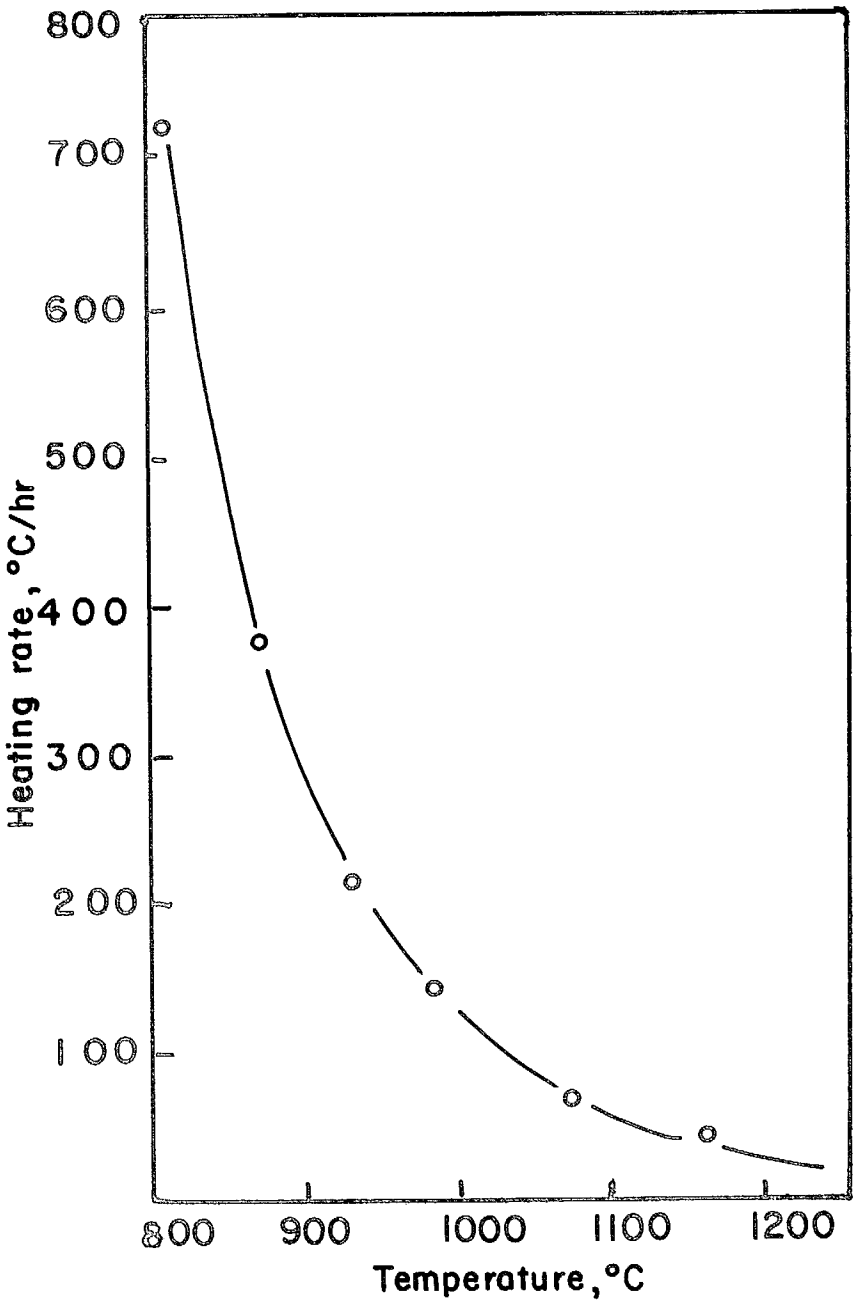

Figure 1. Heating rate of electrical resistance furnace as a function of temperature.

of the metal salts such as the nitrates and to subsequently spray dry the mixture. If the salts decompose at a reasonably low temperature of less than 350°C, it would also be possible to operate a spray drier towards the upper limit of its temperature range so that the solution is simultaneously dried and calcined to the oxide in one process.

Unfortunately, it was not possible to prepare mixtures in the K_2O-MgO-TiO_2 system in this manner because the decomposition temperature is higher than the upper limit of conventional spray-drying equipment. In addition, the nitrates tend to melt at low temperatures rendering them unsuitable for use in the spray drying process. Because of these limitations, the homogeneity that can be developed in aqueous solutions was retained by the alternative technique of flash freezing. In this manner, the desired mixtures could be prepared by very rapidly immobilizing the ions in the frozen solution and subsequently removing the ice by sublimation using a freeze drier to produce a reactive and homogeneous material.

The technique used in the present work was a modification of the normal procedure in that a mixture of both a solution and a suspension were mixed and frozen together. Previous work had shown that it is impossible to successfully freeze dry zirconyl salts using a commercial freeze drier capable of operating down to -40°C because the salt gradually melts[14]. Because of the chemical similarity between these two Group-IV B elements (Zr and Ti), it was assumed that the same difficulty would occur in the present study. Consequently, the process was based on that

used earlier to produce CaO-doped ZrO_2 powders from solutions of the salts[15].

In essence, the titanyl ion was removed from solution by precipitating a finely divided titanium hydroxide. The precipitate was washed to remove soluble salts and subsequently doped with a known amount of $(CH_3.COO)K$ and $(CH_3.COO)_2Mg$ in solution. The resulting slurry was rapidly frozen and successfully dried at -5°C without difficulty. A general outline of the process is given in Figure 2.

Precipitation of Titanium Hydroxide*

Initially, the quantity of NH_4OH required to precipitate $Ti(OH)_4$ from $TiCl_4$ was determined by a potentiometric titration. Twenty millilitres of 99.5% $TiCl_4$ (Anachemia Chemicals Ltd., Toronto) was carefully diluted with 250 mL of distilled water producing a strongly exothermic reaction. The pH was recorded as increments were added of a dilute NH_4OH solution, made by mixing 50 mL concentrated NH_4OH with a sp gr of 0.9 from Allied Chemical Ltd., Pointe Claire, Montreal, in 625 mL distilled water. The results showed that 447 to 454 mL of NH_4OH solution was required to give a pH of 6.5 to 7.0 respectively, i.e., every 20 mL of concentrated $TiCl_4$ needs 35.8 to 36.3 mL of concentrated NH_4OH. The potentiometric curve for this precipitation using the diluted solutions is shown in Figure 3.

From this initial data, it was determined that a 300-g sample having the composition of x equal to 1.8 would require approximately 675 g of TiCl having a density of 1.726, i.e., requiring 391 mL.

---

*The exact composition of the hydrate oxide which is precipated is unknown, but is probably given by the formula $TiO(OH)_2O.nH_2O$. For brevity, the formula $Ti(OH)_4$ has been used throughout this report.

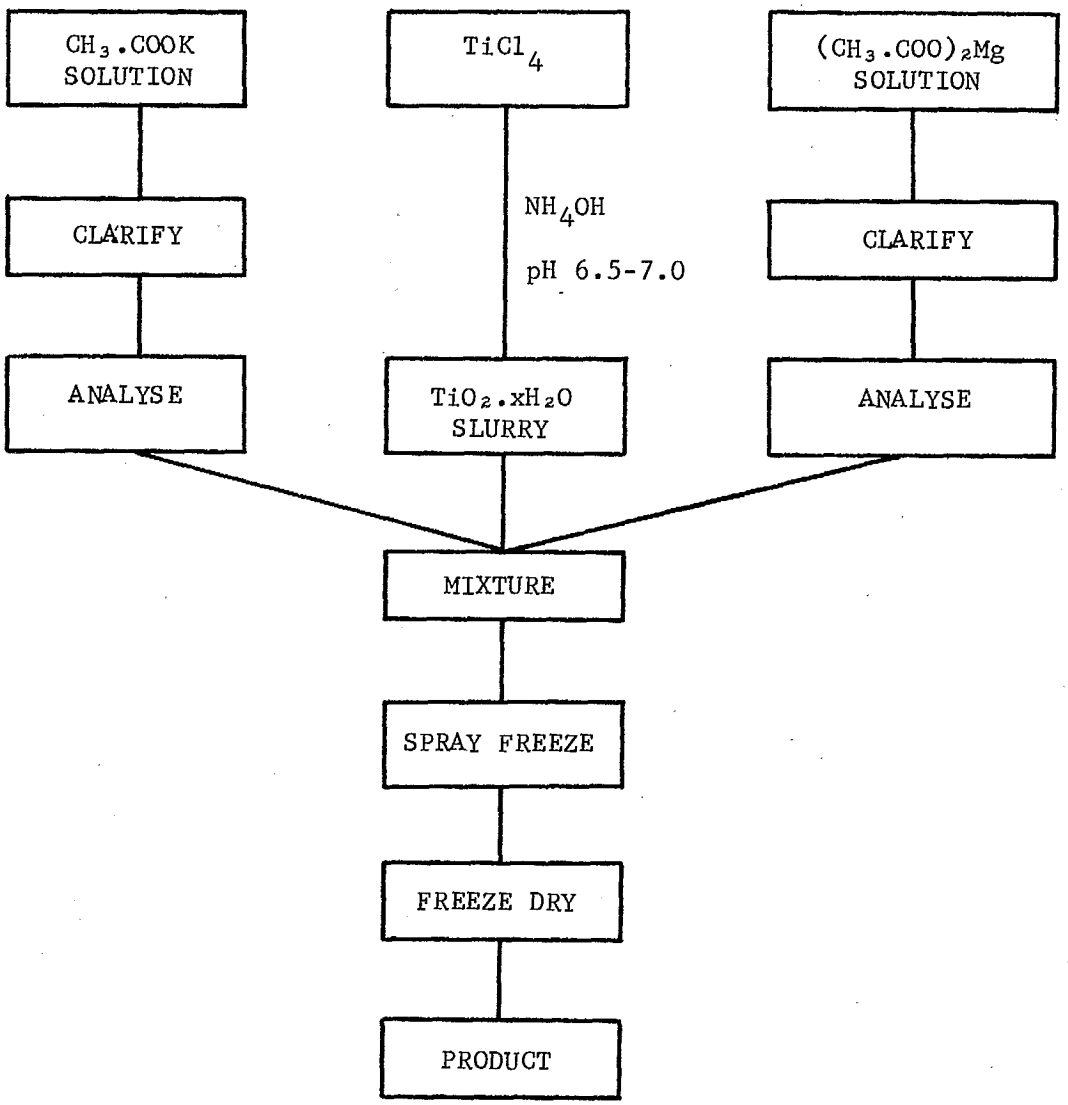

Figure 2. General flow sheet for the preparation of mixtures in the K_2O-MgO-TiO_2 system

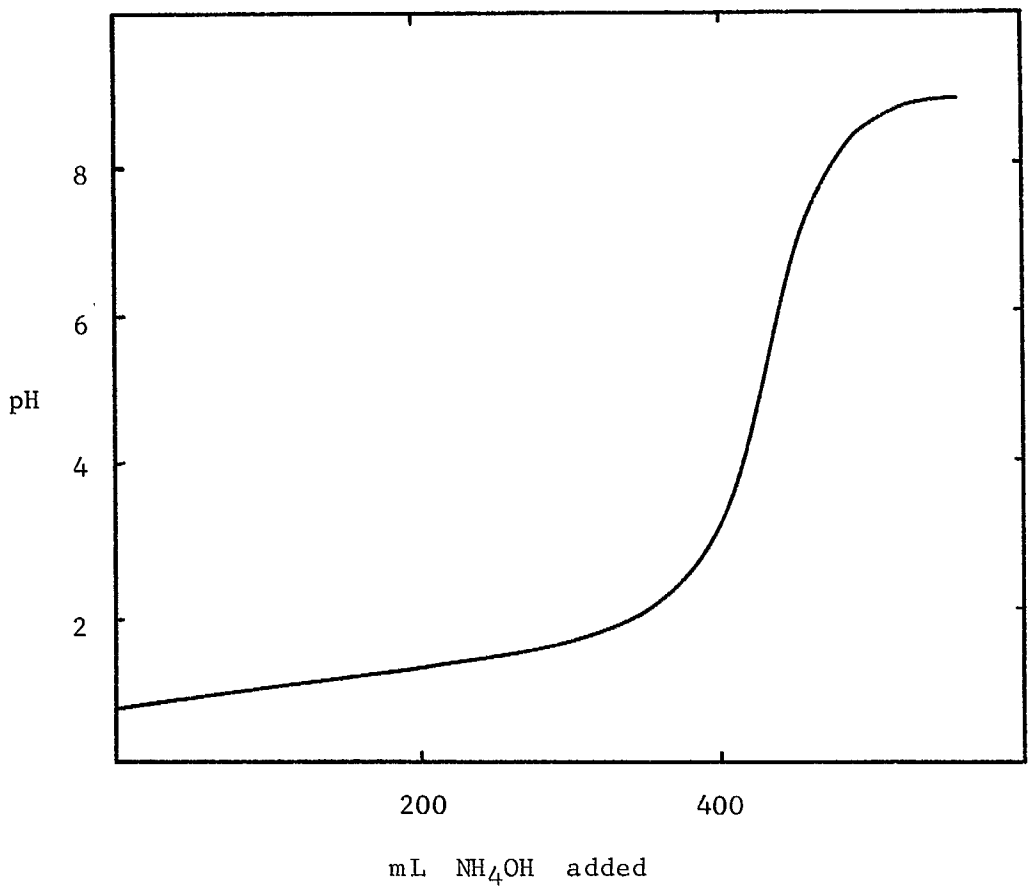

Figure 3. Potentiometric titration of 20 mL of as-received $TiCl_4$.

To avoid compounding any error in the titration data, the full amount of NH_4OH required was not added directly, only 90% of the calculated amount initially, and the remainder added slowly until the pH rose to within the range from 6.5 to 7.0. Consequently, 391 mL of $TiCl_4$ was diluted with 10 L of distilled water and this solution was added slowly to a continuously stirred solution of 650 mL of concentrated NH_4OH in 10 L of distilled water. The pH immediately after mixing was 1.8. Increments of additional diluted NH_4OH solution were added until the pH increased to 6.53 when the slurry was made up to a total of 50 L using distilled water. After standing overnight, the precipitate settled to approximately 13 L indicating that the concentration of the $Ti(OH)_4$ sediment was 2.18 wt %.

The clear supernatant liquor was discarded and the precipitate

subsequently washed with distilled water until the concentration of Cl^- remaining in the stirred slurry was less than 20 ppm.

During the washing stage, it was noticed that the pH of the slurry gradually increased and that above approximately pH 8.5 the slurry was deflocculated sufficiently that the supernatant liquor would not clear on standing. Consequently, the pH was lowered by the addition of HNO_3 until a value in the range of 6.5 to 7.0 was obtained. Approximately 15 washing steps were required to lower the Cl^- concentration to 7 ppm, at which point the settled slurry had a pH of 6.98 and the supernatant liquor a pH of 6.71. Continued washing for an additional 15 cycles gradually lowered the pH of the slurry to 5.84 and of the liquor to 5.85, but the Cl^- concentration remained essentially constant. Presumably the precipitate initially adsorbs both Cl^- and NH_4^+ ions from solution during the precipitation stage: because the $TiCl_4$ was added to the NH_4OH solution, the initial portion of the precipitate would be formed in a considerable excess of NH_4^+ ions. During the initial washing stage, adsorbed ions are gradually removed from the surface making the slurry increase in pH during the first eight washings until the HNO_3 was added. Subsequently, the pH gradually drops after the removal of NH_4^+ due to the use of distilled wash water of pH 5.8.

After the final washing, the supernatant liquor was decanted from the settled precipitate to leave approximately 8 L of slurry, which was stirred vigorously for 2 hr and divided into equal portions by transferring into weighed containers. At the same time, two 25-mL batches of slurry were pipetted into weighed 50-mL platinum dishes. The dishes were dried to constant weight at 110°C, weighed, and ignited to

constant weight at 1000°C and re-weighed. From these data, the quantity of TiO_2 in each container was determined.

Preparation of Potassium and Magnesium Doped Titanates

From the concentration of slurry and the weight of each batch, the number of moles of TiO_2 in each container was determined and the amount of CH_3COOK and $(CH_3.COO)_2Mg$ could be determined as shown in Appendix A.

The salts were added in the form of a mixed solution. In each case, the appropriate amount of acetate was dissolved in water to give a 0.5 molar solution; the two solutions were then mixed and slowly added to the rapidly stirred slurry. The mixture remained very fluid throughout this stage. After standing overnight, the mixture was spray frozen by spraying directly into liquid N_2 using a pneumatic jet operating at 56 to 70 kPa (8 to 10 psi) air pressure and a liquid feed rate of 45 mL/min[16]. The frozen material was finally freeze dried at -10°C for 48 hr under a vacuum of 3.3 to 5.9 x 10^4 Pa (250 to 450 Torr) to produce a white, bulky free-flowing powder.

RESULTS AND DISCUSSION

PART A. CHARACTERIZATION OF RAW MATERIALS

I. Conventionally Ball Milled Raw Materials

Of all the common ceramic raw materials, TiO_2 is probably the most difficult to disperse in the dry state. Even on being shaken in a bottle, it will readily agglomerate into spherical particles ranging from approximately 0.5 mm to 3 cm in

diameter. This property makes it all the more difficult to prepare well-dispersed mixtures and to ensure the development of homogeneous doped titanates. In addition, this characteristic 'stickiness' of the TiO_2 also prevents adequate particle sliding from occurring during the cold-pressing stage of the forming process. Consequently, the agglomerate structure present in the initial powder is retained throughout the subsequent forming and firing stages, resulting in a very inhomogeneous pore distribution in the sintered body. Examples of both types of inhomogeneity - chemical and physical - were observed frequently in the present work.

Figures 4 to 7 show the microstructure developed in compacts made from the ball milled raw materials after firing in air to 1200°C for 15 hr. It can be seen that the microstructure developed in these materials is quite heterogeneous. Irrespective of composition, they all have a discontinuous pore size distribution due to the poor flow characteristics of the material under pressure during the green-forming stage. In all cases, the microstructures reveal the presence of large, very porous, circular areas scattered throughout these materials. Such areas, which may be up to 300 μm in diameter as shown at the left-hand side of Figure 5(a), are thought to be due to the presence of relatively porous but stable agglomerates being formed in the original ball-milling stage. During compaction, these agglomerates are retained intact and during the subsequent firing stage they suffer an abnormally high shrinkage to leave these nearly circular very porous areas. The presence of irregularly

(a) 200 μm

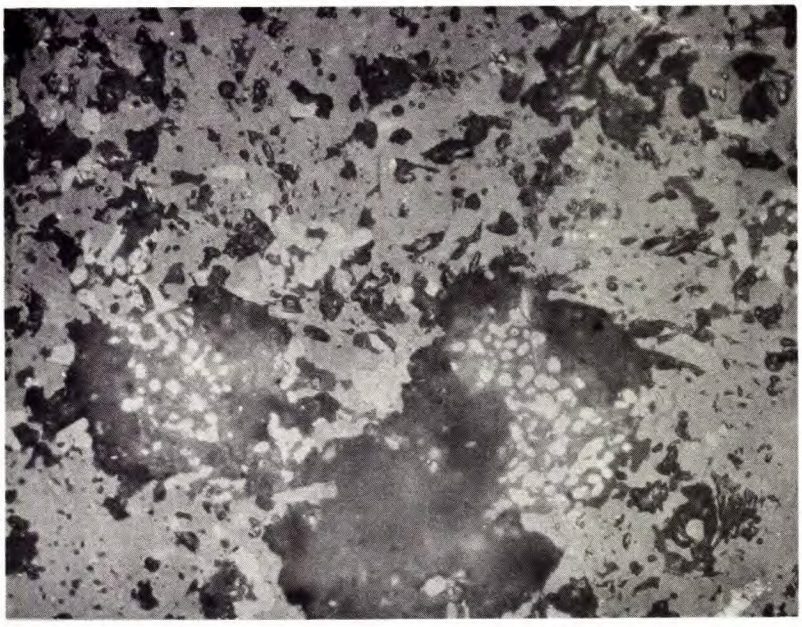

(b) 50 μm

Figure 4. Microstructure developed in compacts of ball milled material fired in air to 1200°C for 15 hr. Overall composition of sample: $0.7K_2O:0.7MgO:7.3TiO_2$, i.e., x equals 1.4.

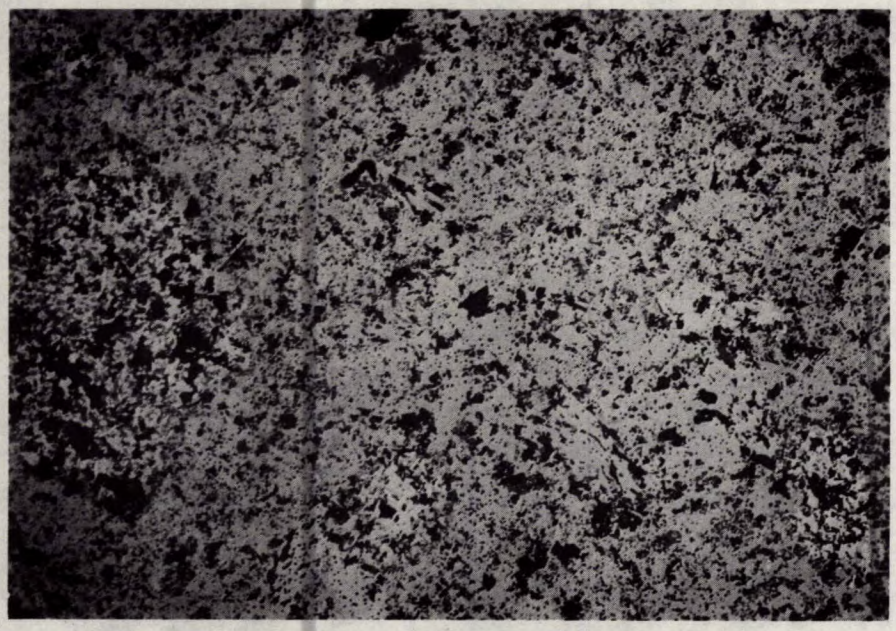

(a) 200 μm

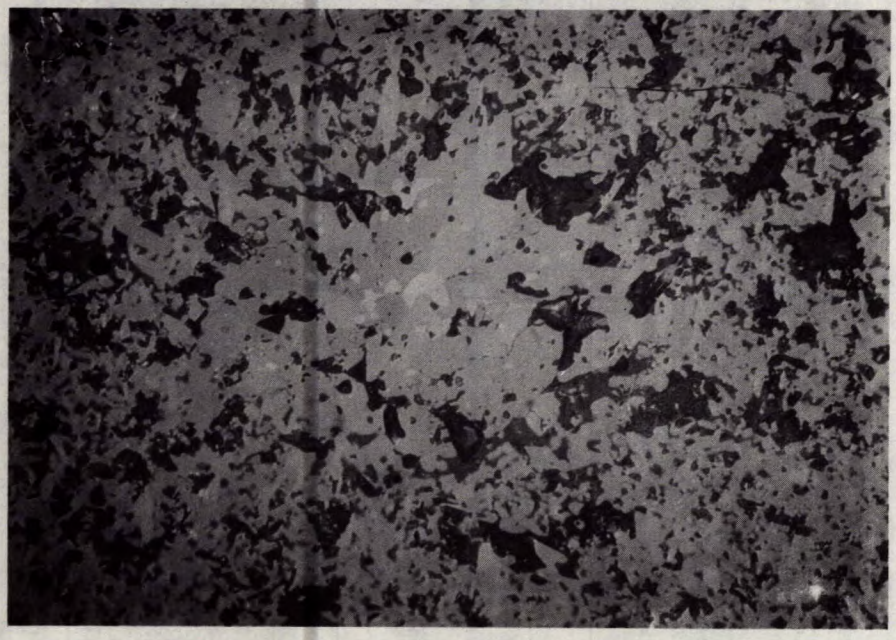

(b) 50 μm

Figure 5. Microstructure developed in compacts of ball milled material fired in air to 1200°C for 15 hr. Overall composition of sample: $0.8K_2O:0.8MgO:7.2TiO_2$, i.e., x equals 1.6.

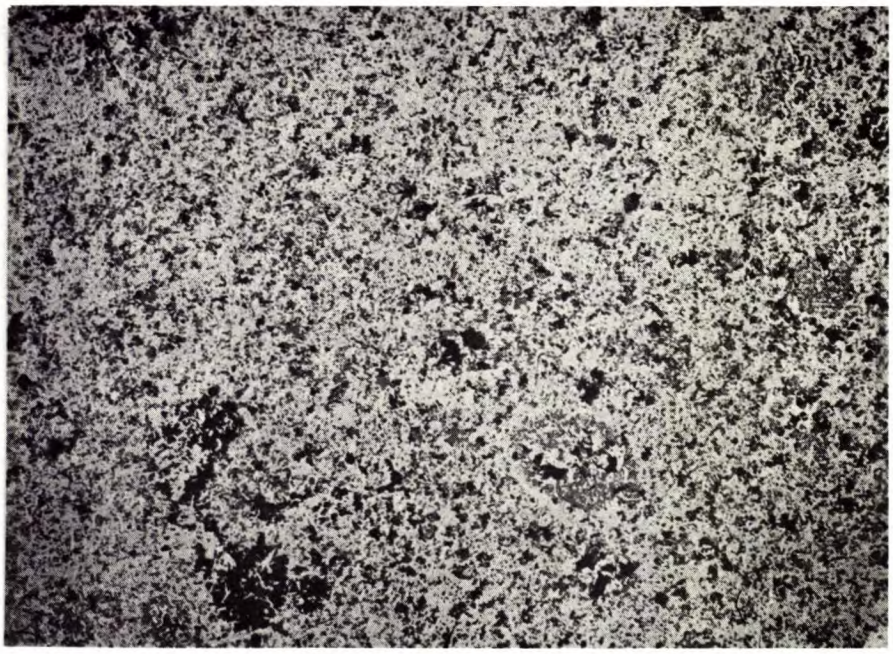

(a) 200 μm

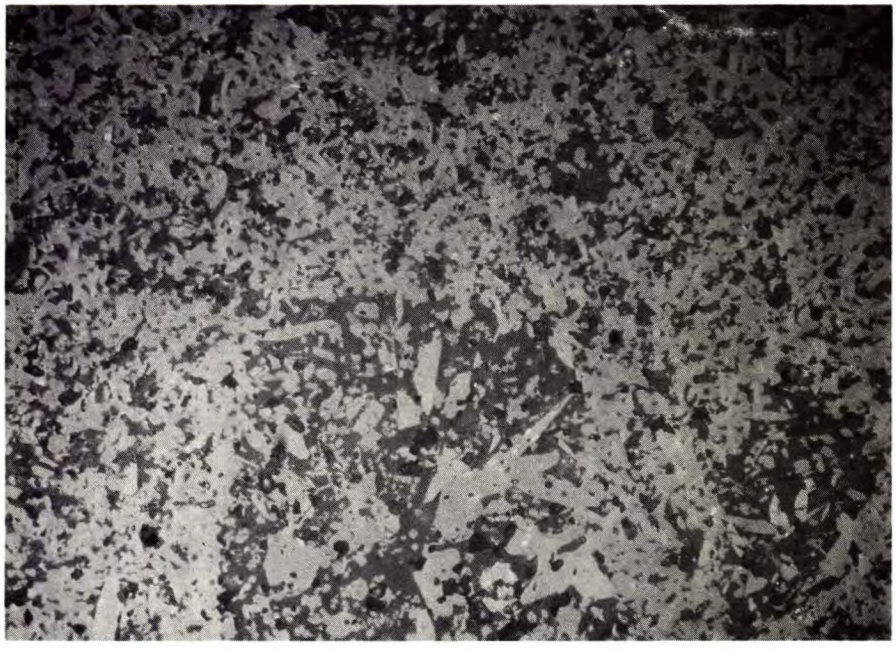

(b) 50 μm

Figure 6. Microstructure developed in compacts of ball milled material fired in air to 1200°C for 15 hr. Overall composition of sample: $0.9K_2O:0.9MgO:7.1TiO_2$, i.e., x equals 1.8.

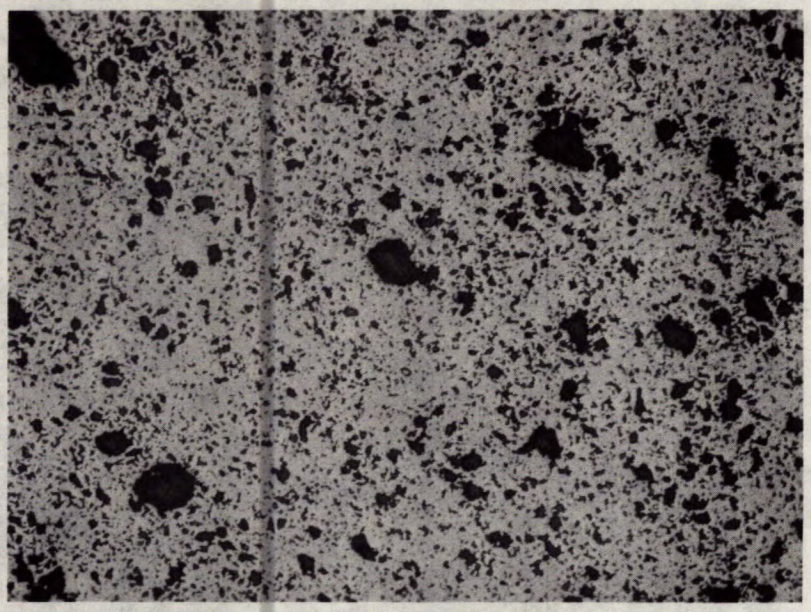

(a) 200 μm

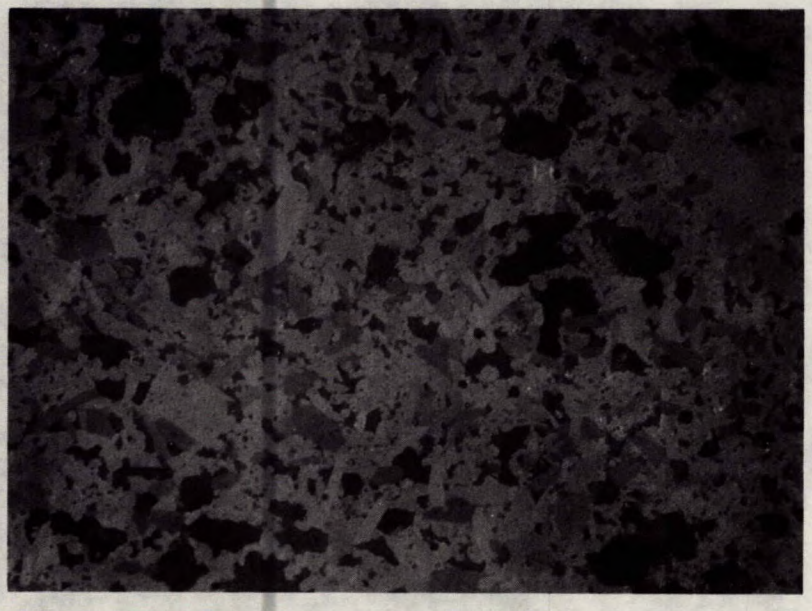

(b) 50 μm

Figure 7. Microstructure developed in compacts of ball milled material fired in air to 1200°C for 15 hr. Overall composition of sample: $K_2O:MgO:7TiO_2$, i.e., x equals 2.0.

shaped pores of approximately 20 μm in diameter further suggests the inability of these materials to flow during the pressing operation to form the body. It is assumed that such pores are the result of particle bridging.

Examination of these materials at high power reveals that the very fine porosity, which lies in the range of approximately 1 μm to 8 μm, is generally situated on the grain boundaries. However, in certain areas such as the central area shown in Figure 5(b), the fine porosity is trapped within the grains themselves suggesting that in this area rapid grain growth has prevented the normally slowly moving grain boundaries from acting as vacancy sinks and eliminating the pores as they were intercepted. It can be seen that this intragranular porosity is also associated with an abnormally large grain size, further suggesting that such areas are the result of discontinuous grain growth.

Although these materials show a physically heterogeneous structure, it is more significant that they are also chemically heterogeneous. The former characteristic could probably be drastically reduced by the use of a suitable lubricant to allow a more uniform structure to be formed during pressing. However, the latter is more difficult to control. Extensive milling would help but it would also introduce undesirable contamination. Examination of the titania-rich composition where x equals 1.4, Figure 4, shows the presence of a highly reflecting second phase (white) and also a third phase (light grey) within the general hollandite matrix (grey). X-ray diffraction confirmed the presence of the high temperature form of free TiO_2 (rutile) as the only additional phase present; the inability to detect the

third phase is presumably due to its much lower concentration.

Unfortunately, it is not possible to reproduce the microstructure realistically in the micrographs shown in Figures 4 to 7. The close similarity in the reflectivity between these phases gives the misleading impression of an apparently chemically uniform microstructure. In reality, the field of view shown in Figure 4(a) is composed of widely dispersed areas of free TiO_2 as rutile, (white), a low concentration of an unknown phase (light grey), the main hollandite-type phase (grey), acrylic mounting resin which has filled the exposed pores (dark grey), and the original closed pores (black).

This heterogeneous microstructure was also developed in the $x = 1.6$ and 1.8 materials. However, both these compositions were devoid of any free TiO_2 and, in addition, the $x = 1.8$ material was also free of the unknown light-grey phase observed in the $x = 1.4$ composition. Consequently, the $x = 1.8$ material was found to be chemically homogeneous - the traces of white shown in Figure 6(b) are believed to be subsurface reflections. A common feature shown by all the compositions was the lath-shaped morphology of the crystals and the tendency to a bimodal size distribution. As a result, the small crystals are approximately 6 μm in length whereas the large crystals are up to 30 μm in length.

The formation of TiO_2 agglomerates during the milling stage is further confirmed by the presence of free TiO_2 exclusively in the circular, porous areas shown in the microstructure of the $x = 1.4$ material, Figure 4(a). A similar microstructure is also developed in the $x = 1.6$ material but the

reflectivity is lower than that of TiO_2 and the X-ray diffraction pattern only showed the presence of a single-phase material. Consequently it is possible that the x = 1.6 material contained areas of TiO_2-rich phase together with the other unknown light grey phase; in each case, these phases are in too low a concentration to be detected by X-ray diffraction techniques. Figure 5(a) contains three areas that are thought to consist of the TiO_2-rich phase: the left hand side 300-μm diameter agglomerate and the two approximately 100-μm diameter areas at the bottom of the micrograph in the centre and right-hand side.

Unfortunately, X-ray diffraction analysis did not identify the additional phases present in these materials. The second phase material present in the x = 2.0 composition and seen as a medium to dark grey phase in Figure 7(b) was present in sufficient quantity to appear in powder diffraction patterns. This material was found to be isostructural with the phase $K_yLi_yTi_{4-y/2}O_8$ recently reported by Roth et al. for the system K_2O-Li_2O-TiO_2 [13]. Although the composition of this phase remains unknown, it probably corresponds to the formula $K_2MgTi_3O_8$.

From the above, it would be concluded that single-phase material can only be formed in an x = 1.8 composition. However ever, it is possible that the chemical heterogeneity observed in both the x = 1.6 and x = 2.0 materials could result from the gradual loss of K_2O during the extended firing cycle. Because these samples retained a considerable amount of open porosity, this loss would not necessarily be confined to the surface layers

Figure 8. As-fired surface of x = 2.0 material showing the development of whiskers.

but would be distributed throughout the whole compact. Densities in the range from 3.02 g/cc to 3.48 g/cc were recorded, i.e., from 82% to 93% of the theoretical density, and dye impregnation confirmed that such values were insufficient to develop a closed-pore system.

Direct evidence for the loss of volatile material from these samples is the gradual development of surface whiskers on extended firing at 1200°C for 24 hr, shown in Figure 8. The tendency to whisker growth increased as x increased, i.e., as the concentration of K_2O in the compact increased. X-ray fluorescence analysis of these whiskers, using the energy

dispersive attachment of the scanning electron microscope, confirmed the considerable increase in the K concentration of the whiskers compared with that of the substrate, Figure 9.

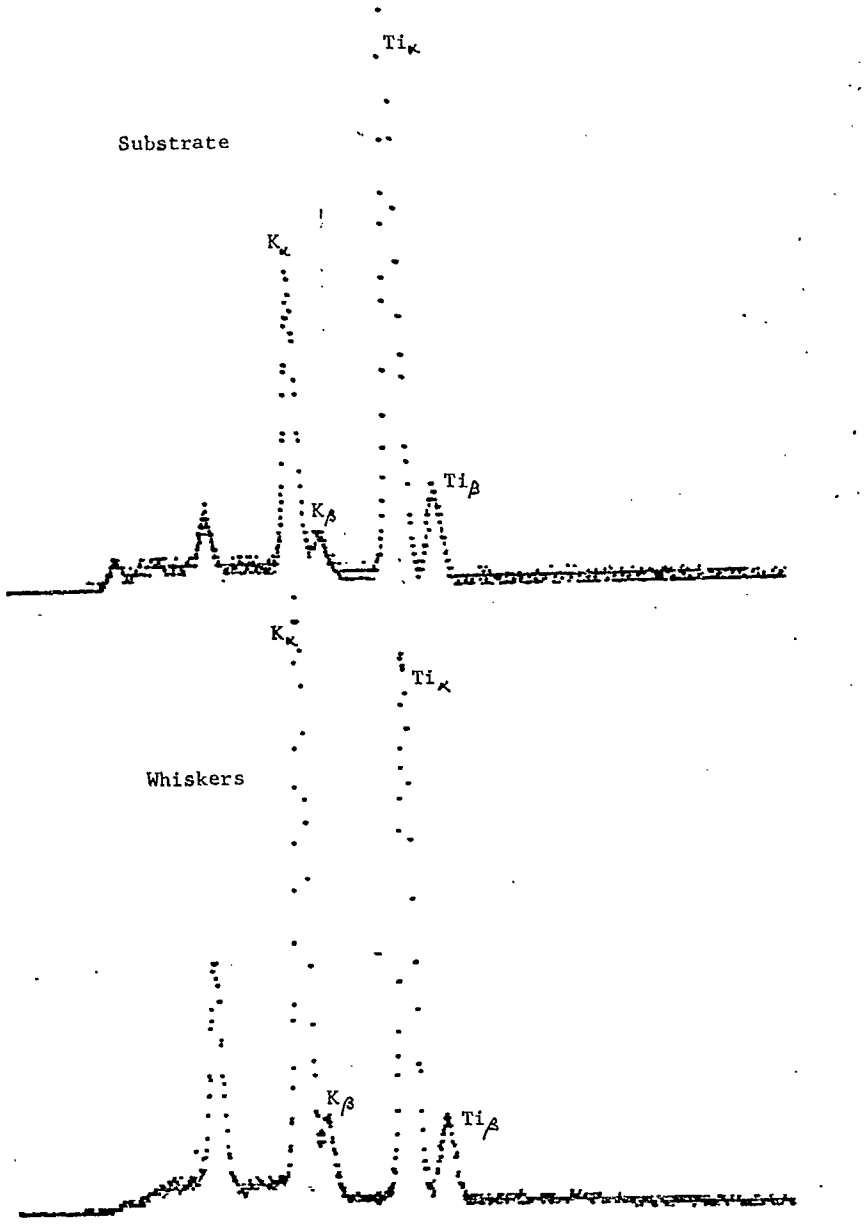

Figure 9. X-ray fluorescence spectra obtained from a sample of $x = 2.0$ material fired in air to 1200°C for 24 hr.

Because of the poor quality of the microstructure developed in these ball milled compositions and the known sensitivity of electrical properties of most materials to structural inhomogeneities, no further examinations were made of these materials.

II. Wet Chemically Prepared Raw Materials

All the as-prepared materials were bulky, free-flowing white powders with a tap density of approximately 0.15 g/cc. In all cases, X-ray diffraction analyses indicated that these powders were amorphous immediately after leaving the freeze-drier.

Thermal Analysis of As-Prepared Materials

Figure 10 shows a thermal gravimetric analysis (TGA) and a differential thermal analysis (DTA) obtained by heating the undoped freeze-dried $Ti(OH)_4$ precipitate in air. The DTA curve indicates an endothermic reaction between approximately 80°C and 250°C and a much less intense exothermic reaction that occurs at approximately 860°C. The low-temperature reaction is also accompanied by a considerable weight loss due to the gradual loss of both physisorbed and chemisorbed water from the sample. A total weight loss of 14.5% was recorded for the freeze-dried powder and all this loss occurred below approximately 500°C. The exothermic reaction at 860°C is probably related to a rapid crystal growth of the TiO_2 but this could not be verified by either optical microscopy or X-ray diffraction analysis.

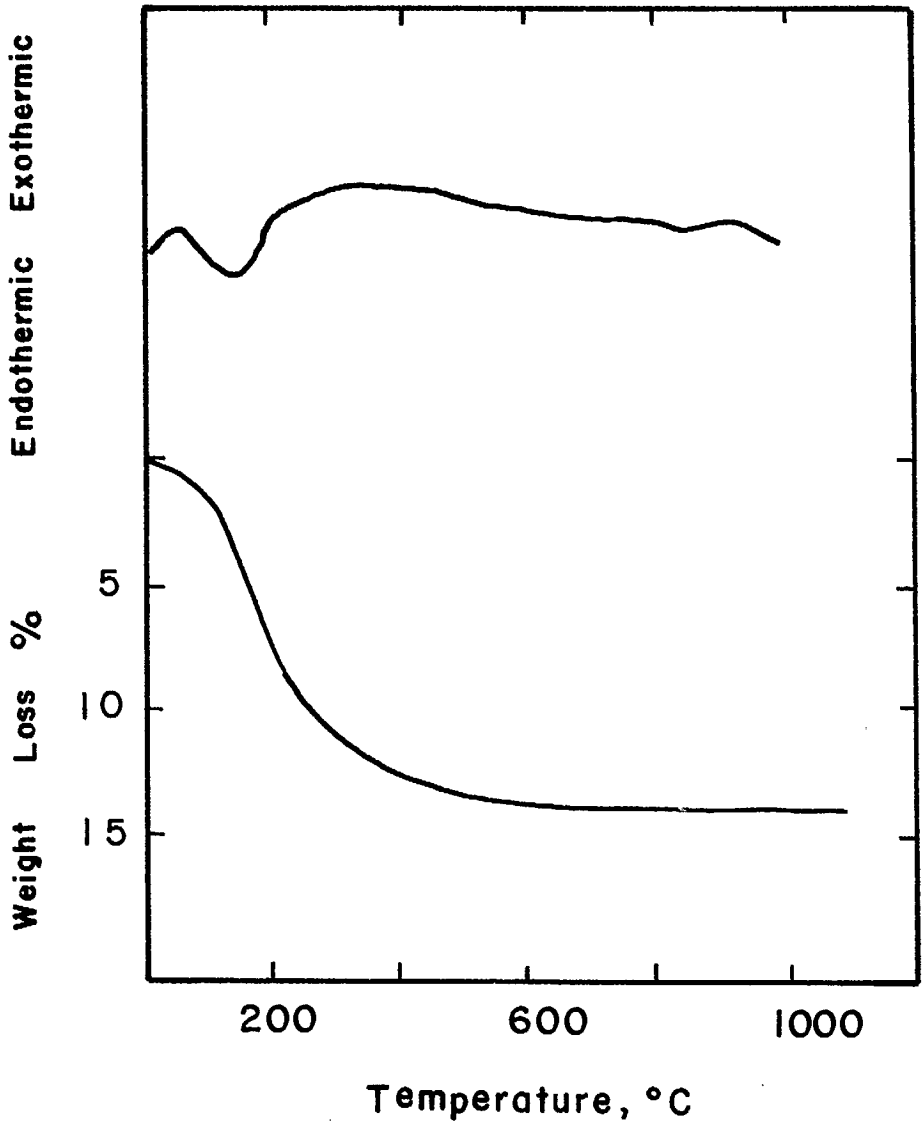

Figure 10. DTA and TGA curves for undoped TiO_2 heated in air.

Figures 11 and 12 show the TGA and DTA data respectively for the various doped materials. Unlike the undoped $Ti(OH)_4$, the weight-loss curve shows two regions of loss: one at approximately 200°C and a second, very sharp weight loss at 360°C to 410°C depending on the composition. The low-temperature loss is also accompanied by an endothermic reaction shown by the DTA. The form of the weight-loss curve between 100°C and 250°C is

similar to that of the undoped TiO_2: in each case the curve appears to be asymptotically approaching a loss of approximately 15%. This, together with the associated relatively weak and broad endothermic peak in DTA, suggests the powders lose water over this temperature interval.

It would be expected that the total weight loss suffered by each powder would increase progressively as the amount of dopants added to the TiO_2 is increased, i.e., as x is increased. However, this would depend on the TiO_2 itself having a constant weight loss in all cases and this is not so. As shown in Figure 11, the weight loss up to 200°C can vary from as little as 5% to over 11%. In addition, the magnitude of the loss is also seen to be independent of composition up to this temperature whereas at temperatures above 200°C the additional loss is directly dependent on the composition. Clearly, the amount of sorbed water on the TiO_2 component of each composition is variable.

At slightly higher temperatures, between approximately 225°C and 325°C, the form of the DTA curve becomes dependent on composition. With increasing values of x there is a trend to develop a second endothermic peak at approximately 300°C; this peak coincides with the sudden weight loss of these materials as shown by the TGA curves of Figure 11. Consequently, it is assumed that this behaviour is due to the decomposition of the amorphous $DH_3.COOK$ and $(CH_3.COO)_2Mg$ components.

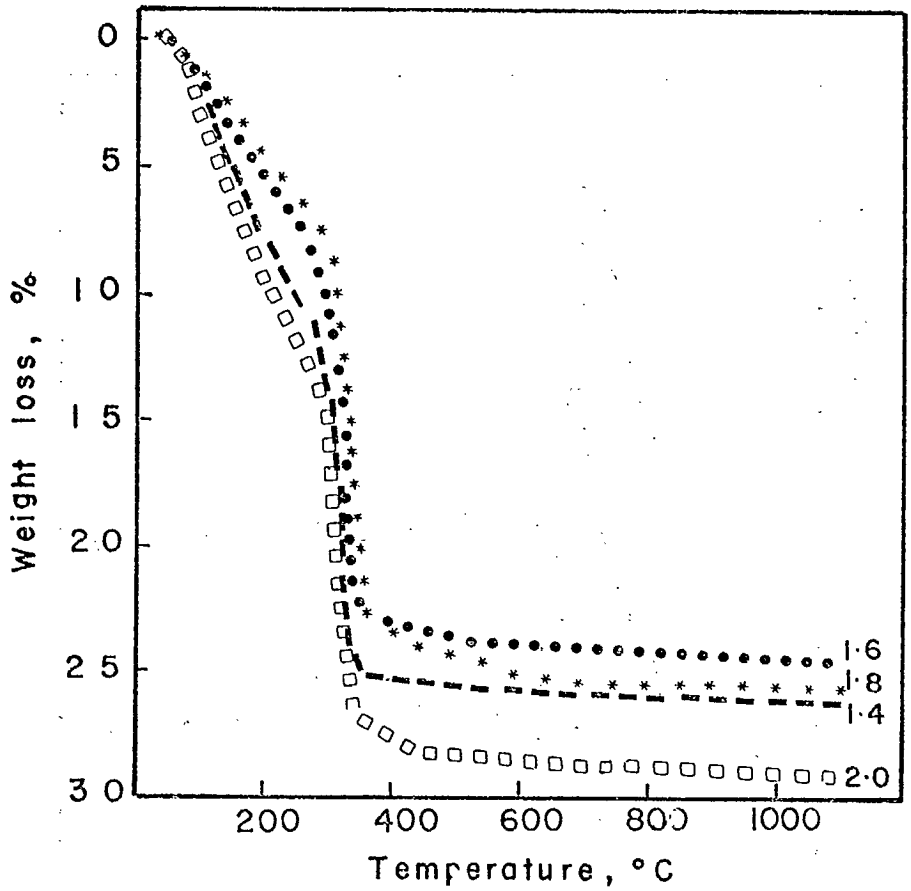

Figure 11. TGA curves for doped, freeze-dried materials heated in air at 6°C/min.

With a further increase in temperature into the range of 375°C to 425°C, all the materials undergo a strongly exothermic reaction. The temperature of this reaction tends to increase with increasing concentrations of K and Mg. For example, in materials having a composition in which x = 1.4, this reaction occurs at approximately 375°C, increasing to 395°C when x = 1.6 and 405°C when x = 1.8 and finally becoming 400°C when x = 2.0. With a progressively increasing temperature up to 1000°C, two other exothermic reactions occur - the first being recorded in DTA as a weak and broad peak centred at 600°C and the second as a weak but sharp peak at 780°C. Both these reactions occur at

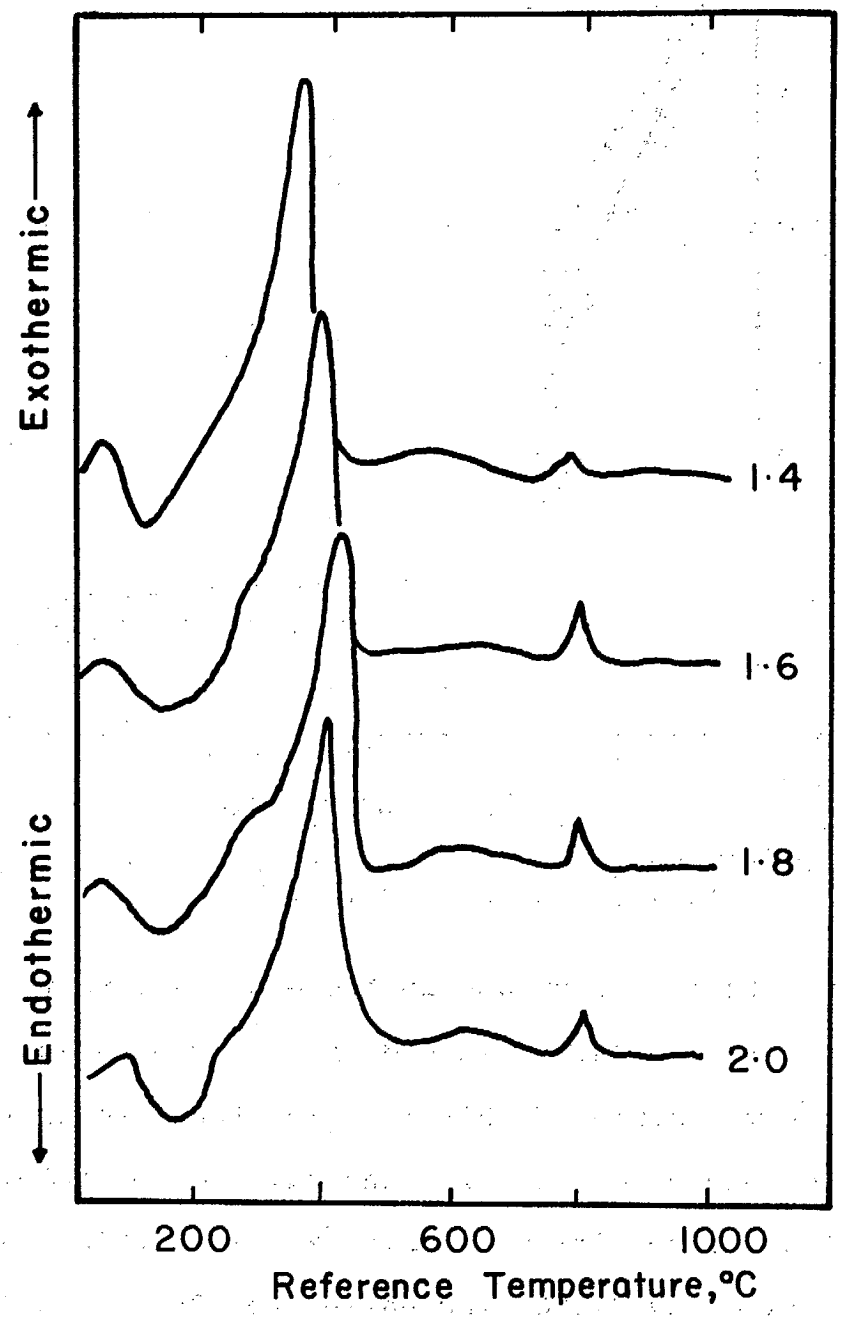

Figure 12. DTA curves for doped, freeze-dried materials heated in air at 12°C/min.

a temperature that is composition dependent, although the temperature increase with increasing values of x is very small.

To further examine the behaviour of these materials during calcination, a series of samples of each composition was prepared by calcining a small quantity of the as-prepared material for 1 hr in air at 225°, 325°, 500°, 600°, 700°, 760°, 810°, 900°, and 1000°C. These temperatures were selected in an attempt to determine the origin of the peaks in the DTA curves. Each sample was examined using X-ray diffraction analysis techniques.

X-ray Diffraction Analyses

All analyses were conducted on the powdered calcines using a Guinier-DeWolff focusing camera as it is inherently more sensitive than a non-focusing diffractometer yet it retains approximately the same angular dispersion (1° 2θ/4 mm of film for the camera; slightly less for the diffractometer). The main disadvantage in using a Guinier camera is that it does not record diffraction data at 2θ angles greater than approximately 90° and hence no information can be obtained from the 'back-reflection' region where minor changes in lattice spacings due to compositional changes or strain effects are more readily observed. Unfortunately, the diffraction patterns produced by the hollandite materials calcined at intermediate temperatures are very weak and hence it was not possible to obtain any pattern from the back-reflection region using either a diffractometer or a Debye-Scherrer camera both of which are capable of

recording diffraction patterns over essentially the full range of 2θ from zero to 180°. For this reason, no data could be obtained on the changes in the lattice parameters of the hollandite phase that may probably occur with increasing temperature.

Diffraction patterns of the various calcines were obtained using Fe-filtered Co K-alpha radiation. Minor changes in the patterns as the calcination temperature increased were readily shown in the derived diffractograms produced by microdensitometer scans of the photographic films. For the purposes of presentation in this report, the operating conditions of the densitometer were so chosen to give maximum attenuation of the recorded peak heights and the minimum of dispersion of the pattern. Under these conditions, most of the weak patterns produced by the materials calcined below 600°C actually appear to be amorphous in their diffractograms shown in Figures 13 to 16.

It can be seen from these figures that none of the materials develops any extensive degree of crystallinity at temperatures much below 700°C. However, even below this temperature, there are important differences in the phase composition of each material that are not completely lost even on subsequent sintering to 1200°C for 3 hr. In the as-prepared state, the powders are essentially amorphous. However, the $x = 1.4$, 1.6 and 1.8 materials also contain low concentrations of poorly crystalline anatase (TiO_2). On heating to 225°C, this condition continues but, in addition, a low concentration of $(COOK)_2$ is also developed in the $x = 1.6$ and 1.8 materials.

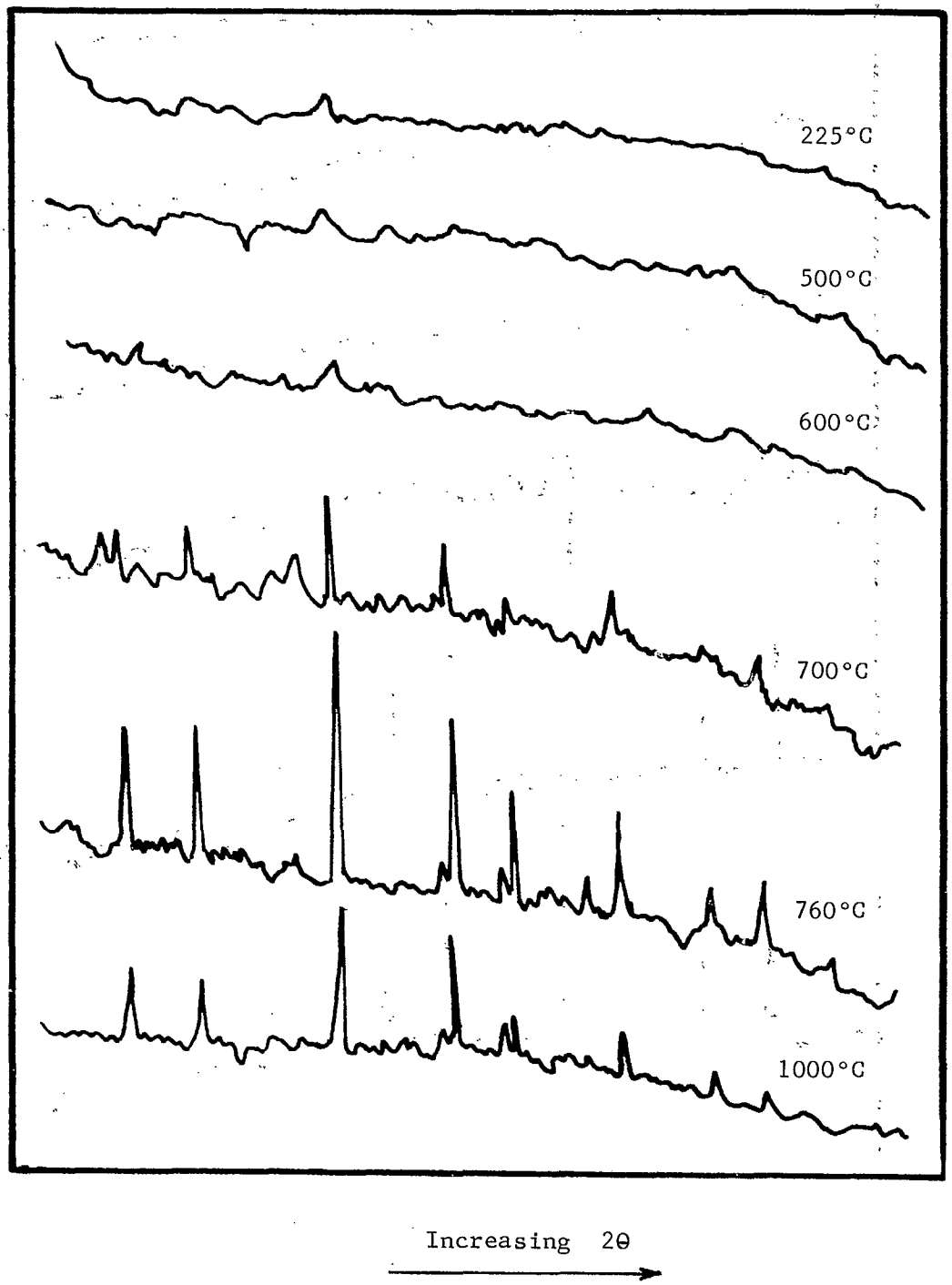

Figure 13. X-ray diffraction patterns of as-prepared x = 1.4 material after heating in air for 1 hr at the temperatures indicated.

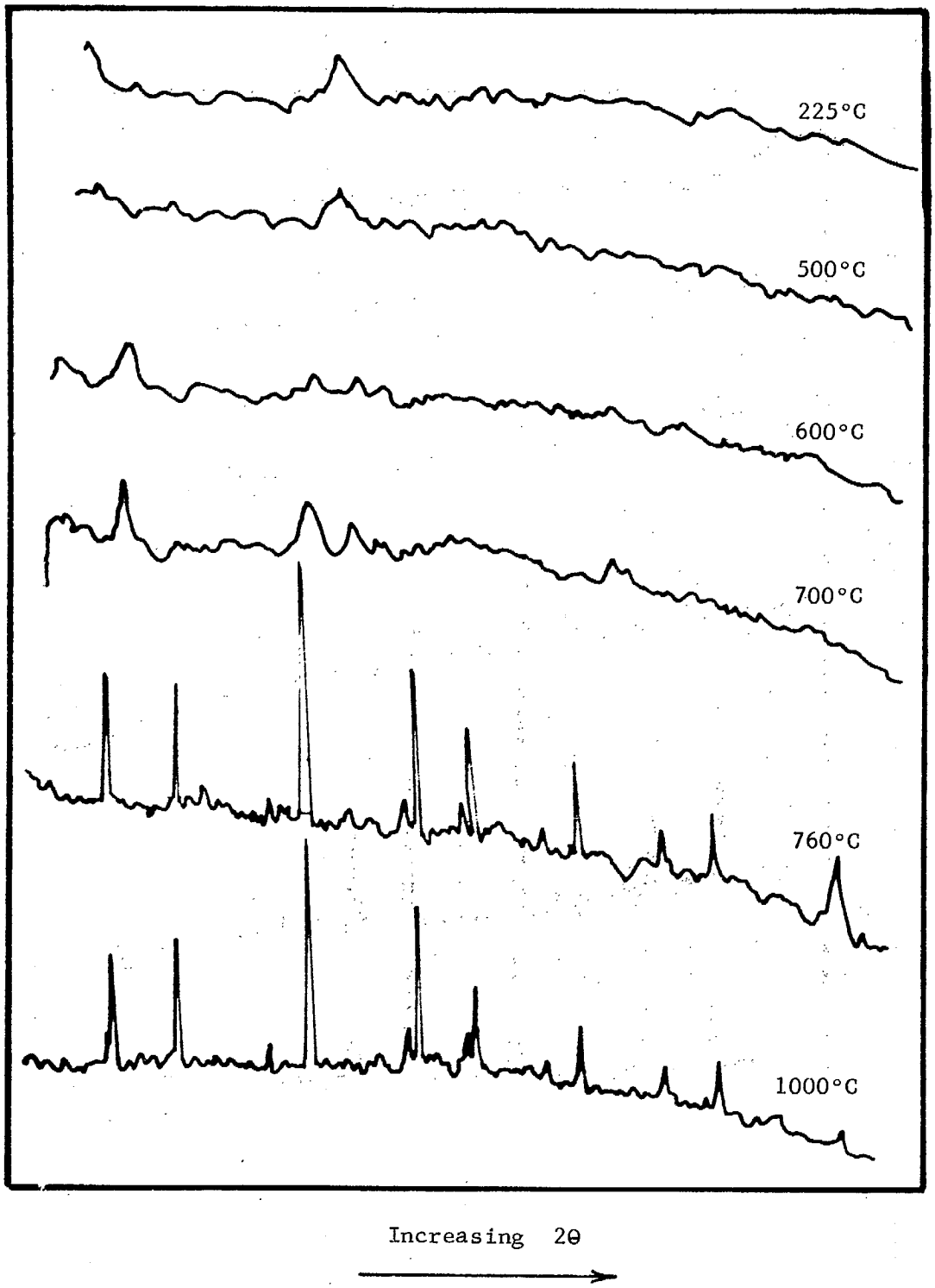

Figure 14. X-ray diffraction patterns of as-prepared $x = 1.6$ material after heating in air for 1 hr at the temperatures indicated.

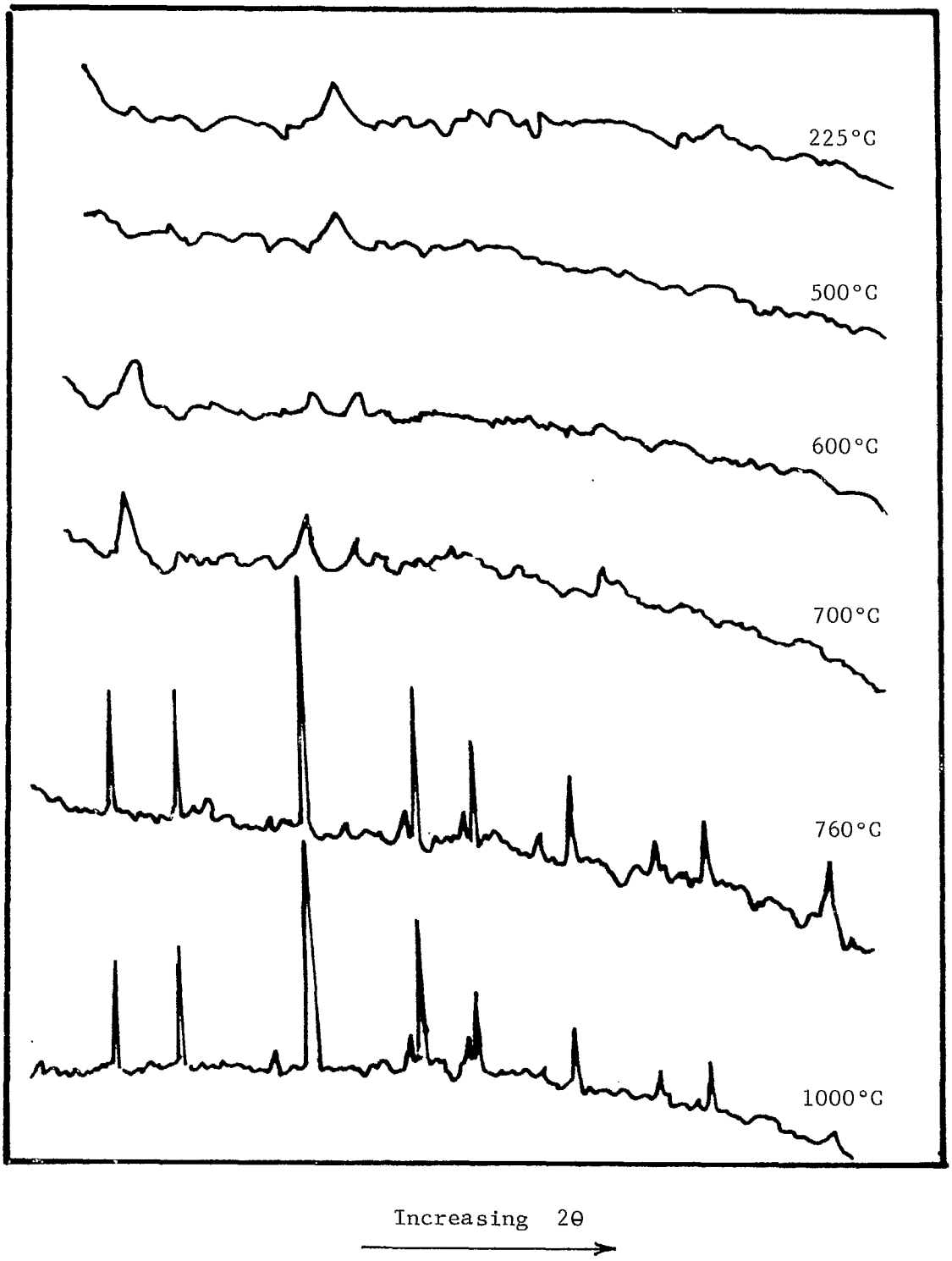

Figure 15. X-ray diffraction patterns of as-prepared x = 1.8 material after heating in air for 1 hr at the temperatures indicated.

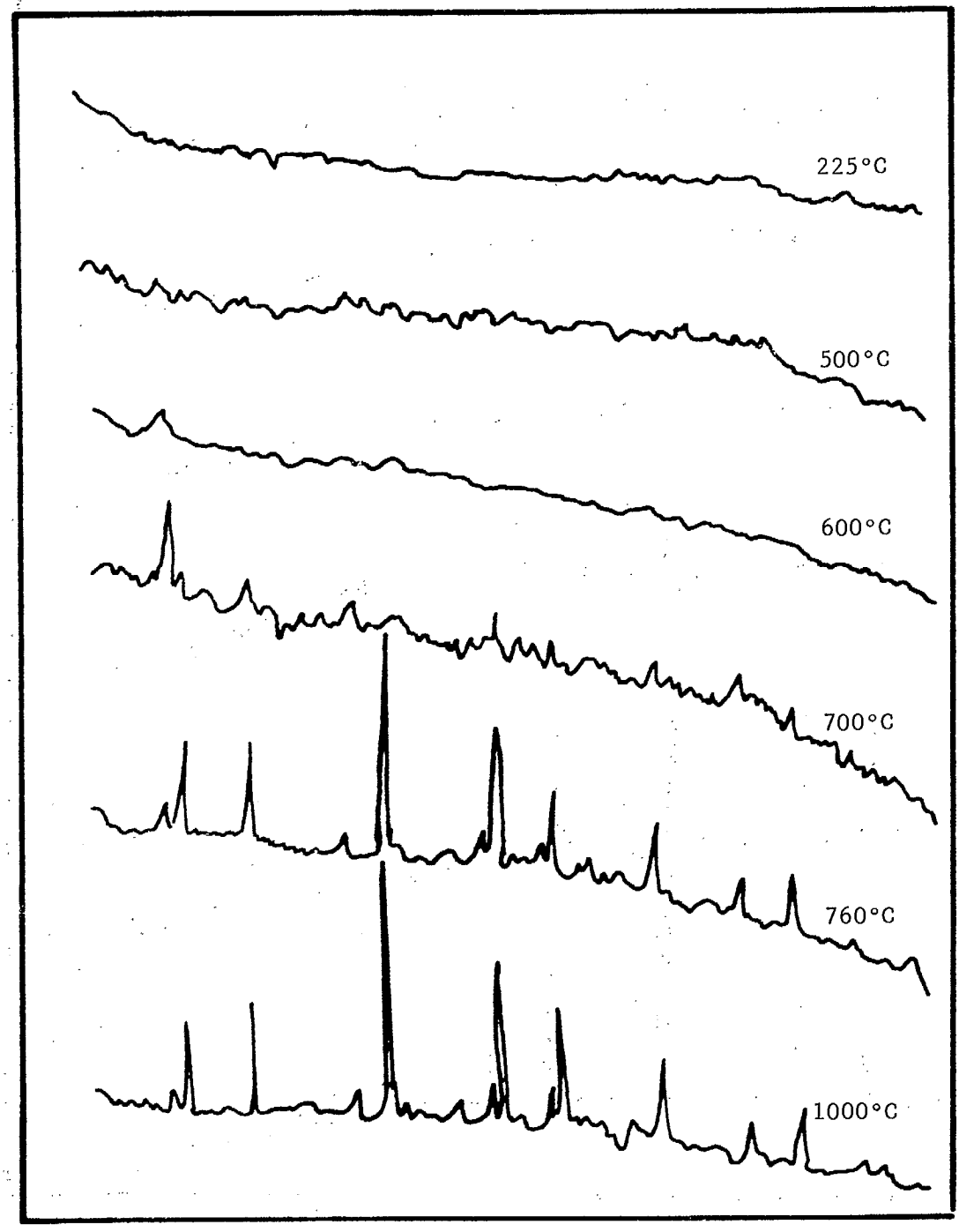

Figure 16. X-ray diffraction patterns of as-prepared x = 2.0 material after heating in air for 1 hr at the temperatures indicated.

On further heating to 325°C, the second-phase $(COOK)_2$ is also developed in the x = 2.0 material - the x = 1.4 composition remains unchanged with only the low concentration of anatase. This behaviour is consistent with the sudden weight loss by these materials at this temperature shown in Figure 11 and the development of an endothermic reaction in the DTA curves shown in Figure 12.

It is surprising that such a considerable weight loss can occur without any significant phase change. For example, it might be expected that the CH_3COOK component, which is present in the as-prepared materials in an amorphous state, would first crystallize, which is an exothermic reaction without any weight loss, then decompose to the oxalate at a higher temperature, which is an endothermic reaction with a weight loss, and finally decompose to the oxide which is an endothermic reaction with weight loss. On the presence of the other reagents, the oxide might possibly form an intermediate potassium titanate. Similarly, the amorphous $(CH_3.COO)_2Mg$ component might be expected to first crystallize, then decompose to the carbonate, and finally decompose to the oxide as the temperature is progressively increased. Yet neither of these reaction paths are followed. On the contrary, the Mg component remains amorphous throughout the calcination stages until it is incorporated into a crystalline titanate at temperatures above 600°C and, other than the development of two weak diffraction lines indicating the presence of a low concentration of the oxalate, the same is true of the K component.

Calculation shows that if such a step-wise decomposition of the two acetate components were to occur, a weight loss of approximately 5% would occur at each step which is well within the limits of detection of the thermobalance used in the present work. Consequently, it must be concluded that both the K and Mg components decompose directly to their respective oxides at approximately 355°C, otherwise the TGA curves would show additional regions of weight loss with associated endothermic reactions being recorded in DTA. This behaviour is similar to that reported elsewhere, in which most of the decomposition of a $(H.COO)_2Ca$ dopant, added to a $ZrO(OH)_2$ precipitate in a manner similar to that used in the present work, was found to proceed directly to the oxide with only 3-5% of the dopant decomposing via the expected carbonate intermediate[4]. However, one of the main differences between the behaviour of the CaO-doped ZrO_2 and the hollandites produced in the present work is that the former materials crystallized immediately on decomposition of the dopant to give a solid solution of CaO in ZrO_2 whereas the latter remain essentially amorphous on decomposition at 325°C. It is probable that this is due to the overriding influence of the ZrO_2 and TiO_2 in each case: the former crystallizes readily on heating, irrespective of the concentration of dopant, whereas the latter does not. As a result, the adsorbed amorphous K and Mg acetates decompose at 325°C to oxides on the surface of TiO_2 that remains largely amorphous, and because of the intimate mixing achieved by the wet-chemical technique used to prepare the initial powder, the dopant oxides are too dispersed to form

discrete, crystalline, second and third phases.

Examination of materials calcined at 500°C showed the continued presence of a low concentration of poorly crystalline anatase in all compositions together with a second-phase K- and Mg-rich titanate, having the composition $K_2MgTi_3O_8$, developed in the x = 1.8 and 2.0 materials. The low concentration of $(COOK)_2$ developed at lower temperatures in the x = 1.6, 1.8 and 2.0 materials is no longer present. This apparent transition of the crystalline K phase to an amorphous state that occurs on heating the x = 1.4 and 1.5 materials would initially suggest that a liquid phase has been formed. However, the absence of any clinkered material in these calcines rules out that possibility and suggests that the low amount of crystalline material decomposes and enters into solid solution with the TiO_2. Unfortunately this could not be verified using X-ray diffraction analysis.

On reaching 600°C, all the materials are composed of a mixture of a low concentration of anatase and $K_2MgTi_3O_8$. The largely amorphous character of all the compositions at this temperature is shown clearly in the diffractograms of Figures 13 to 16. With a further increase to 700°C, all compositions develop a significant degree of crystallinity although the diffraction peaks remain broad, indicating a small crystallite size of probably less than 30 nm (300 Å) In addition, all compositions now consist of the high-temperature form of crystalline TiO_2 (rutile) rather than anatase together with the first evidence of crystalline hollandite. The $K_2MgTi_3O_8$ phase is also present in all compositions. With an

increase in temperature to 760°C, $K_2MgTi_3O_8$ persists in the 1.8 and 2.0 materials, whereas it reacts with the TiO_2 in the $x = 1.4$ and 1.5 materials to form more hollandite, as shown by the marked increase in the intensity of the diffraction peaks. No apparent change occurs between 760°C and 810°C (of exothermic peak in DTA at 780°C), the $x = 1.4$ and 1.6 materials consist of rutile and hollandite and the $x = 1.8$ and 2.0 materials are composed of these two phases with the addition of $K_2MgTi_3O_8$.

By 900°C, the phase assemblage becomes stable to further increases in temperature. The $x = 1.4$ material is found to have insufficient K and Mg to dope all the TiO_2 present and form single-phase hollandite and consequently a two-phase mixture of hollandite and rutile persists. In the $x = 1.6$ and 1.8 materials, only single-phase hollandite remains whereas in the $x = 2.0$ material, an excess of K and Mg is present and thus a two-phase mixture of hollandite and $K_2MgTi_3O_8$ is retained. A summary of the overall reactions that occur in each material during heating is given in Figure 17.

Comparison of the X-ray data with the DTA data fails to reveal the origin of the exothermic reactions at approximately 400°C and 780°C. The weak broad exothermic peak at 600°C appears to be due to the nucleation and slow growth of the hollandite phase. It was thought initially that the 400°C exotherm was due to the sudden nucleation of a crystalline phase and that the second exotherm at 780°C was due to its subsequent growth at a higher temperature. Such a reaction would be analogous to that known to occur on heating kaolin between 1000°C and

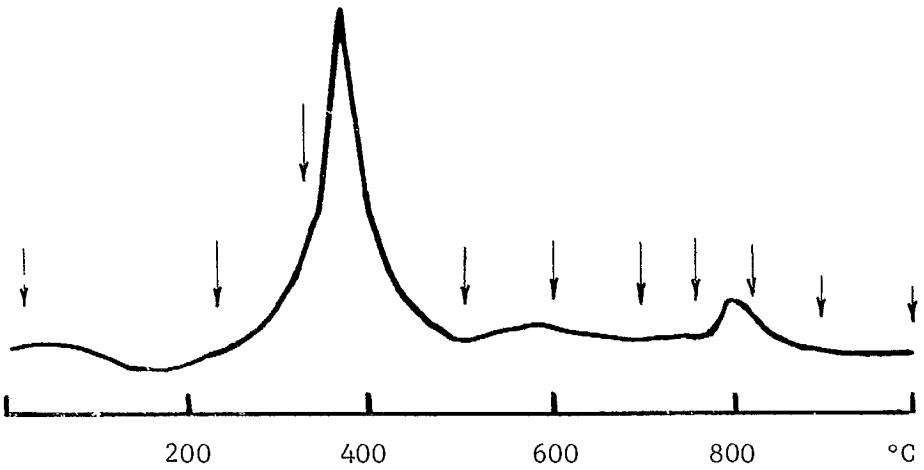

Compn.	25°C	225°C	325°C	500°C	600°C	700°C	760°C	810°C	900°C	1000°C
1.4	A	A	A	A	AK	RKH	RH	RH	RH	RH
1.6	A	AO	AO	A	AK	RKH	RH	RH	H	H
1.8	A	AO	AO	AK	AK	RKH	RKH	RKH	H	H
2.0	?	AO	AO	AK	AK	RKH	RKH	RKH	KH	KH

Figure 17. Summary of the reactions occurring during the calcination of freeze-dried materials.

A - TiO_2 (anatase) R - TiO_2 (rutile)

K - $K_2MgTi_3O_8$ O - $(COOK)_2$

H - $K_xMg_{x/2}Ti_{8-x/2}O_{16}$ (hollandite)

1200°C. A strong and sharp exotherm at 1000°C is due to the nucleation of a low concentration of mullite whereas the weaker and broader exothermic peak at 1200°C arises from the extensive crystal growth of the mullite. Unfortunately, the X-ray data could not support this hypothesis: the origin of the peaks remains unexplained.

PART B. FABRICATION AND CHARACTERIZATION OF SINTERED MATERIALS

It has been shown elsewhere that freeze-dried ceramic powders can be satisfactorily fabricated and sintered to 99% density[4]. However, to develop such high-density materials, the initial powder must be well dispersed, i.e., the original spherical morphology of the as-prepared powder or the calcined powder must be eliminated (Figures 18a, 18b resp.). Depending on the strength of these powder agglomerates, this morphology may be destroyed during the cold-pressing stage of fabrication when the material is subjected to pressures of typically 35 to 140 MPa (5000 to 20,000 psi) to form the initial green compact. Alternatively, the agglomerates may be strong enough to survive through the green-forming stage yielding an unsuitable microstructure that will not sinter to high density. In this case, the agglomerates must be dispersed prior to pressing by ball milling the powder in a suitable liquid which may also contain dissolved powder lubricants and binders. However, contrary to expectation, the present materials were found to sinter to densities greater than 95% without dispersing the powders prior to pressing.

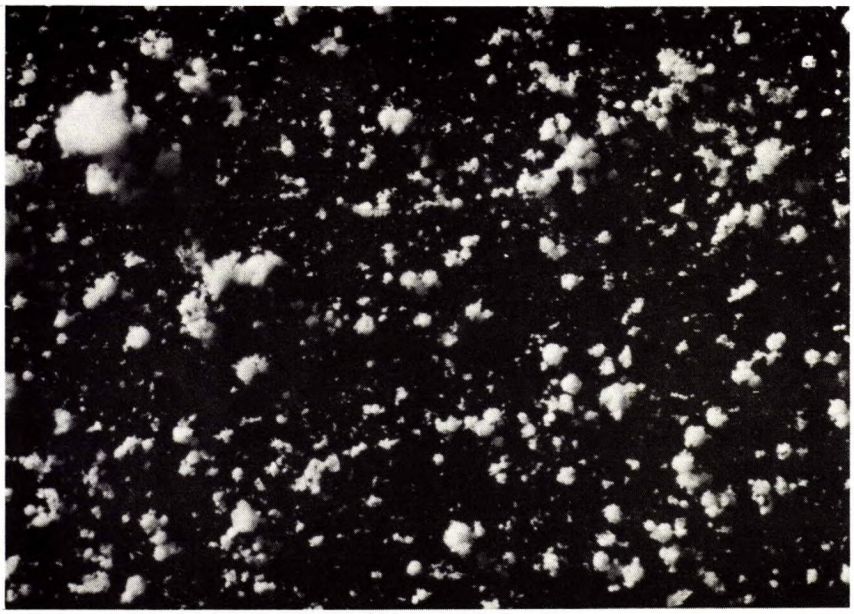

(a) 500 μm

(b) 500 μm

Figure 18. Samples of x = 1.8 material viewed in oblique illumination

(a) As-prepared material
(b) Calcined in air for 1 hr at 825°C.

Effect of Temperature on Density

Calcination Temperature

One of the more important variables in powder processing prior to forming and sintering is the powder calcination temperature. In this pre-sintering stage, the powders are heated to a temperature that is high enough to produce the equilibrium phase assemblage characteristic of the sintered material, thus eliminating all volatile material from the powder without allowing the powder to sinter extensively. Previous work with a variety of freeze-dried powders has shown that satisfactory sintered bodies can readily be produced using calcined powder having a specific surface area between 10 and 20 m^2/g.

It can be appreciated that the choice of calcination termperature is a compromise between a high temperature to ensure the development of a fully reacted powder, but which has a much reduced free surface area and hence a much reduced free energy and a reduced driving force for densification, and a low temperature that will retain a high surface area, but may not lead to the complete removal of volatiles.
Consequently, a series of initial experiments were conducted to determine the effect of calcination temperature on the final sintered density of cold-pressed compacts. For this purpose, samples of each composition were calcined in air for 1 hr at 825°C and 1100°C. These temperatures were selected to examine the effect of low and high calcination temperatures on densification. Both temperatures are adequate to give fully reacted powders, as shown in Figure 17, but the

surface area will be significantly reduced at the higher temperature.

The bulk density of small compacts 1.27 cm (0.500 in.) in diameter and 3 mm (0.125 in.) in height, uniaxially cold pressed in a steel die at 70 MPa (10,000 psi) and subsequently fired in air for 3 hr at 1200°C, is shown in Figure 19. It can be seen that the lower calcination temperature usually leads to the development of the higher density product after sintering. In addition, it can be seen that there is a trend to lower fired densities as the initial powder becomes richer in K and Mg, i.e., as x increases.

Considering the minimal treatment given these materials, the fired densities are surprisingly high. The theoretical density of $x = 1.6$ material has been reported to be 3.69 g/cc[12] and it can be seen that a bulk density of 3.63 g/cc was obtained for the present freeze-dried material of the same composition, i.e., a relative density of approximately 98.4%. Because of these unusually high fired densities obtained using powders that had been calcined at 825°C, all subsequent work was conducted using materials calcined at this temperature.

Sintering Temperature

Clearly, the other major variable in developing high-density sintered material is the firing temperature. To determine the effect of different sintering temperatures, a series of samples of $x = 1.6$ and 1.8 compositions were cold pressed at 70 MPa using powders calcined for 1 hr in air at 825°C and subsequently fired in air for 3 hr at temperatures of 1150°, 1175°, 1200° and 1225°C. The results are shown in Figure 20. It can be seen that

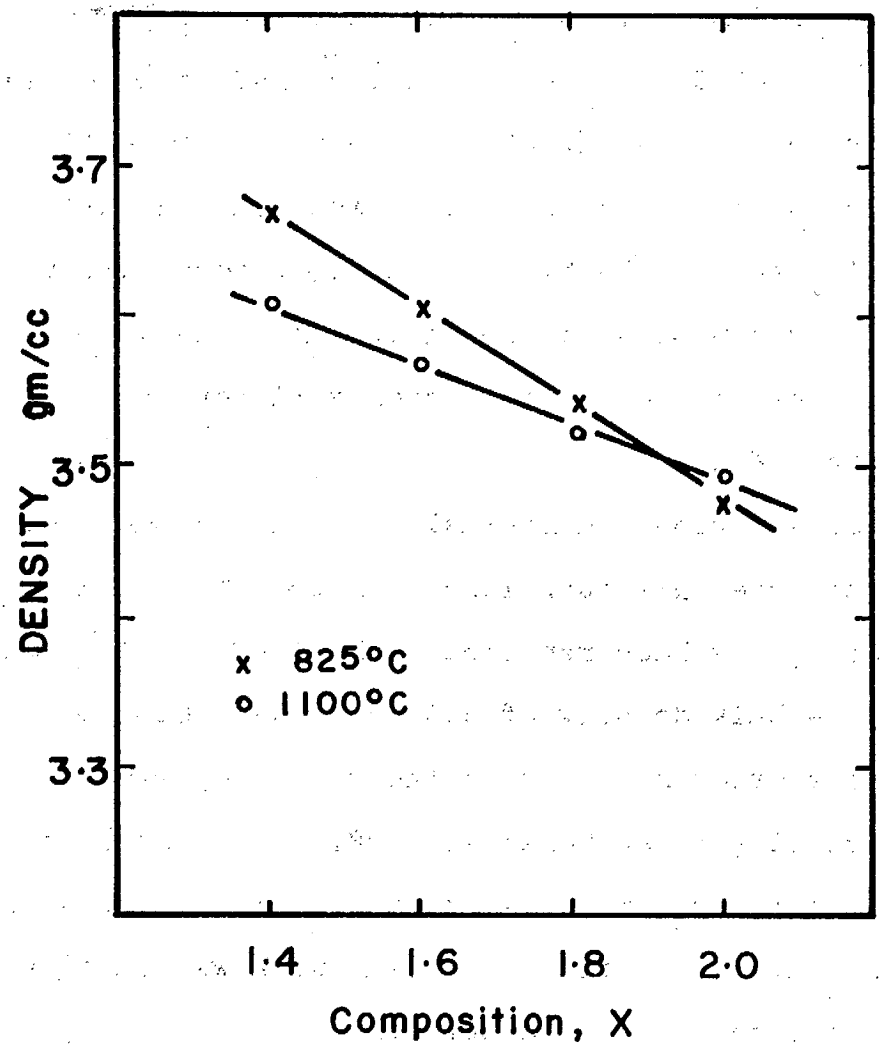

Figure 19. Variation of sintered density with composition for material calcined in air for one hr at the temperatures indicated.

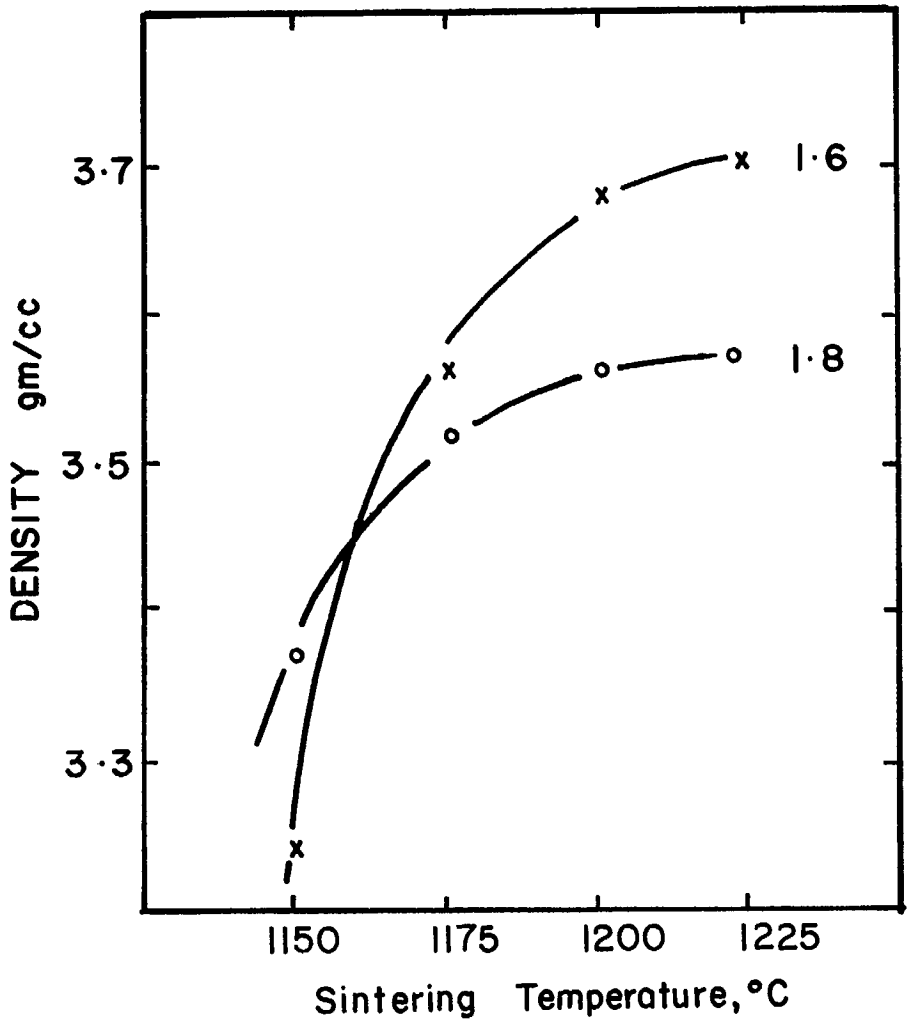

Figure 20. Variation of fired density with temperature for the compositions x = 1.6 and 1.8. Samples were fabricated using material calcined at 825°C for 1 hr.

there is a marked increase in density with temperature for both compositions. In addition, it can be seen that the density of the x = 1.6 material is higher than that of the x = 1.8 samples above approximately 1175°C, which is in agreement with the data of Figure 19.

Although the data presented in Figures 19 and 20 indicate that these materials can be readily formed and sintered to high density, it would be inaccurate to suggest that these data are precise. To minimize the amount of material used, small samples were used, and because of the inherrent increase in error with progressively smaller samples, the precision of the data in Figures 19 and 20 is $\pm$ 0.10 g/cc, i.e., the relative density of the 1.6 material is 98.4% $\pm$ 3.0%.

To obtain more precise data, a series of samples was formed to have a diameter of 3.8 cm (1.5 in.) and a height of approximately 1 cm (0.45 in.). Because of their much larger size, these samples were formed using a modified technique to minimize possible density gradients developing during pressing. For each composition, it was desirable to produce discs having a minimum diameter of 2.54 cm (1 in.) and a height of 6 to 8 mm (0.23 to 0.31 in.) after sintering to a relative density of 95% or more - samples having this geometry were required to determine the thermal properties of these materials as a function of temperature and composition[17]. Consequently, the appropriate amount of powder calcined at 825°C for 1 hr was first blended with approximately 15 wt % of a 5 wt % polyvinyl alcohol-in-water mixture by spraying, using a hand-operated spray gun. The powder was then transferred to a

steel die 3.8 cm (1.5 in.) in diameter and compressed by hand under a total load of approximately 40 kg. Subsequently, the powder was removed from the die and granulated through a 16-mesh screen. The product was then formed into a disc by uniaxially pressing at either 35 or 70 MPa and finally isostatically pressed at 210 MPa. The operating conditions of the forming stage and the results obtained are given in Table 1. It was decided to use the higher pressure of 70 MPa to initially form the discs in order to reduce the diametrical shrinkage that occurs on isostatic pressing, hence the final fired diameter would be larger than that produced by discs formed uniaxially under a pressure of only 35 MPa.

Assuming a theoretical density for the x = 1.6 and 1.8 compositions of approximately 3.70 g/cc[12], it can be seen that the relatively large discs were formed to a green density of 54%. By comparison with a variety of other freeze-dried ceramic raw materials, this is an extremely high value. For example, freeze-dried zirconia and spinel powders commonly develop 25-30% theoretical density on pressing small discs 1.27 cm (0.5 in.) in diameter by 2mm (0.08 in.) thick) of the as-dried powder and only after dispersing by ball milling in alcohol containing dissolved powder lubricants and binders and subsequently spray-drying can the green density be increased to over 50% on isostatically pressing at 210 MPa[15].

Because of this high initial density, it was decided that it would be unnecessary to first disperse the calcined powders prior to pressing. This opportunity to use the calcined

TABLE 1

Development of Cold-Pressed Discs of Freeze-Dried Hollandite Powders

Compn.	P_u*	PVA**	Diam. cm	Thickness cm	Wt g	D_u*** g/cc	P_i*	Diam. cm	Thickness cm	Wt g	D_i*** g/cc
1.5	35	25	3.836	1.171	21.60	1.61	210	3.530	1.105	21.59	1.99
1.6	35	12	3.836	1.182	21.80	1.61	210	3.540	1.120	21.89	1.98
1.7	70	18	3.838	1.092	21.72	1.73	210	3.620	1.062	21.77	1.99
1.8	70	18	3.836	0.992	22.21	1.96	210	3.691	0.970	22.24	2.14

* P_u and P_i – Pressure in MPa used in uniaxially (u) and isostatically (i) pressing samples.

** PVA – Concentration of polyvinyl alcohol-water mixture used to bind powder in wt %. Used a solution concentration of 5 wt%, hence samples contained between 1.25 wt % and 0.6 wt % of actual PVA on a dry-weight basis.

*** D_u and D_i – Bulk density of uniaxially and isostatically pressed discs.

powders directly avoided the risk of contamination that would probably occur in any wet dispersion process; it also avoided the further loss of material that inevitably occurs during the spray-drying process. Consequently these materials were fabricated with the minimum of exposure to inorganic contaminants - the only significant contact being with the steel die used to form the samples prior to isostatic pressing in an evacuated rubber bag. Despite this contact with steel, none of the samples displayed any surface discolouration after firing indicating a very low contamination of the surface, or no contamination at all. In any case, to prepare the fired discs for the measurement of thermal and electrical properties, the samples were first diamond machined to the appropriate geometry prior to measurement, which removed between 1 mm and 3 mm of material from all surfaces.

Because relatively thick samples were being formed for a subsequent examination of the thermal properties of these materials, it was essential that the binder be removed very slowly from the green-pressed discs prior to the firing cycle to avoid laminations and other microstructural defects from forming. DTA of calcined powder containing polyvinyl alcohol (PVA) showed that the endothermic reaction that accompanies the carbonization and burnout of this particular binder occurs most strongly at approximately 340°C with a minor reaction at 470°C, Figure 21. Consequently, for convenience and to also meet the need for a low-temperature burnout, the samples were placed in a 5-cm (1.96-in.) diameter Pt-wound tube

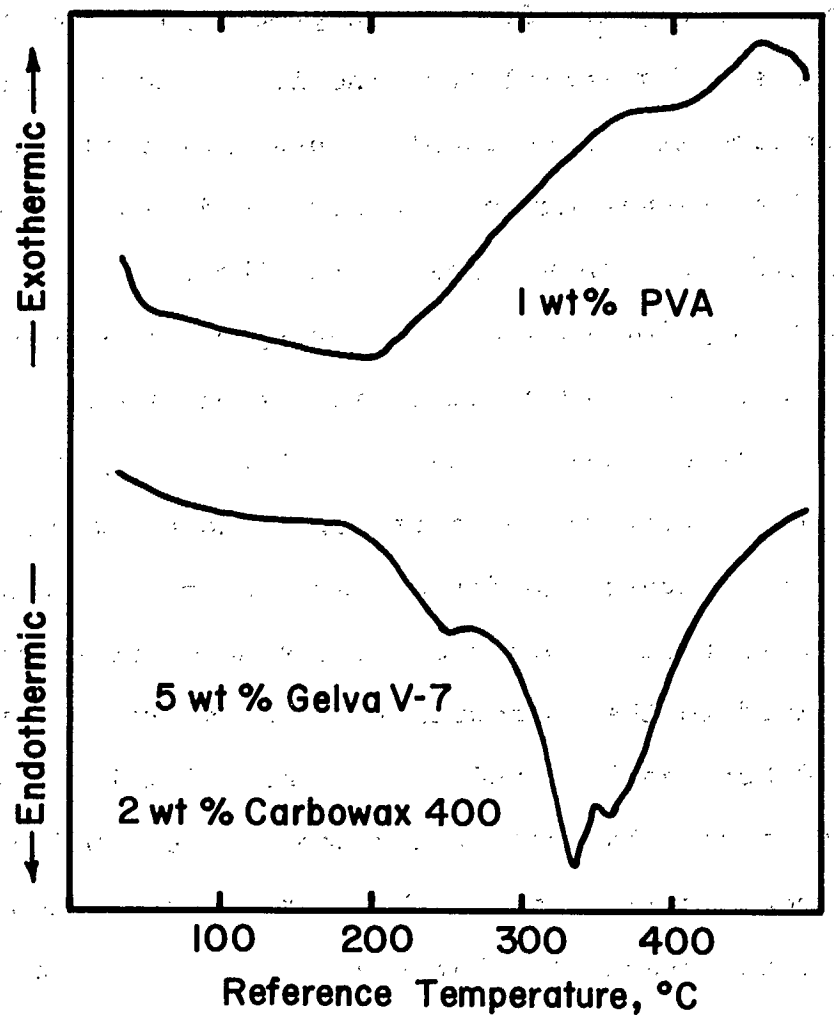

Figure 21. DTA curves of calcined powders containing binder. Concentrations given on a dry-weight basis.

furnace that was heated overnight using a constant power input such that the heating rate was a maximum of 7°C/min at room temperature, decreasing to approximately 1°C/min at 340°C (PVA burnout temperature) and becoming zero at approximately 420°C after 16 hr. Although the samples were heated in a static ambient atmosphere and the tube furnace was horizontal, thus essentially removing convection currents, this procedure was adequate to remove all traces of organic material. TGA of samples so treated showed no additional weight loss below 1000°C.

Hot-stage Microscopy

Prior to actually firing the full-size samples, the sintering behaviour of each composition was determined by firing small samples in air using a Leitz Heating Microscope type IIA-P which is capable of operating in air up to 1750°C. The construction and operation of this equipment has been described elsewhere[18]. The small samples used in the heating microscope were fragments taken from the isostatically pressed large discs, i.e., they were irregularly shaped chips containing PVA binder, but because of their very small size, it was not necessary to first remove the PVA as they had a high surface area-to-volume ratio.

The small samples were heated in an essentially static air atmosphere at 6°C/min in the microscope. The projected image of the sample was photographed at approximately 100°C intervals as the temperature was raised to the melting

point of the material. In this manner, a series of photographs was obtained showing the progressive shrinkage of the sample with increasing temperature. Typical results are shown in Figure 22.

To measure the shrinkage of the samples, the photographic negatives were first enlarged and the areas of the projected image in each print were determined in arbitary units by weighing each cut-out of the silhouette. Assuming the photographic paper was of uniform thickness, the progressive weight change of each print is directly proportional to the progressive area change. Hence, the relative linear shrinkage of the irregularly shaped samples can be determined by measuring the relative change in the square root of the print weight. The results obtained in this manner are shown for each composition in Figure 23.

It can be seen that there is no consistent pattern in the behaviour of the powders as the concentration of K and Mg is increased. Both the magnitude of the shrinkage and the temperature at which shrinkage commences are independent of composition. However, the data do show that sintering starts at approximately 1000°C and, under conditions of constant heating, it continues up to 1400°C. In all cases, the samples were slightly grey after heating to this temperature indicating that the samples were probably losing oxygen and becoming non-stoichiometric.

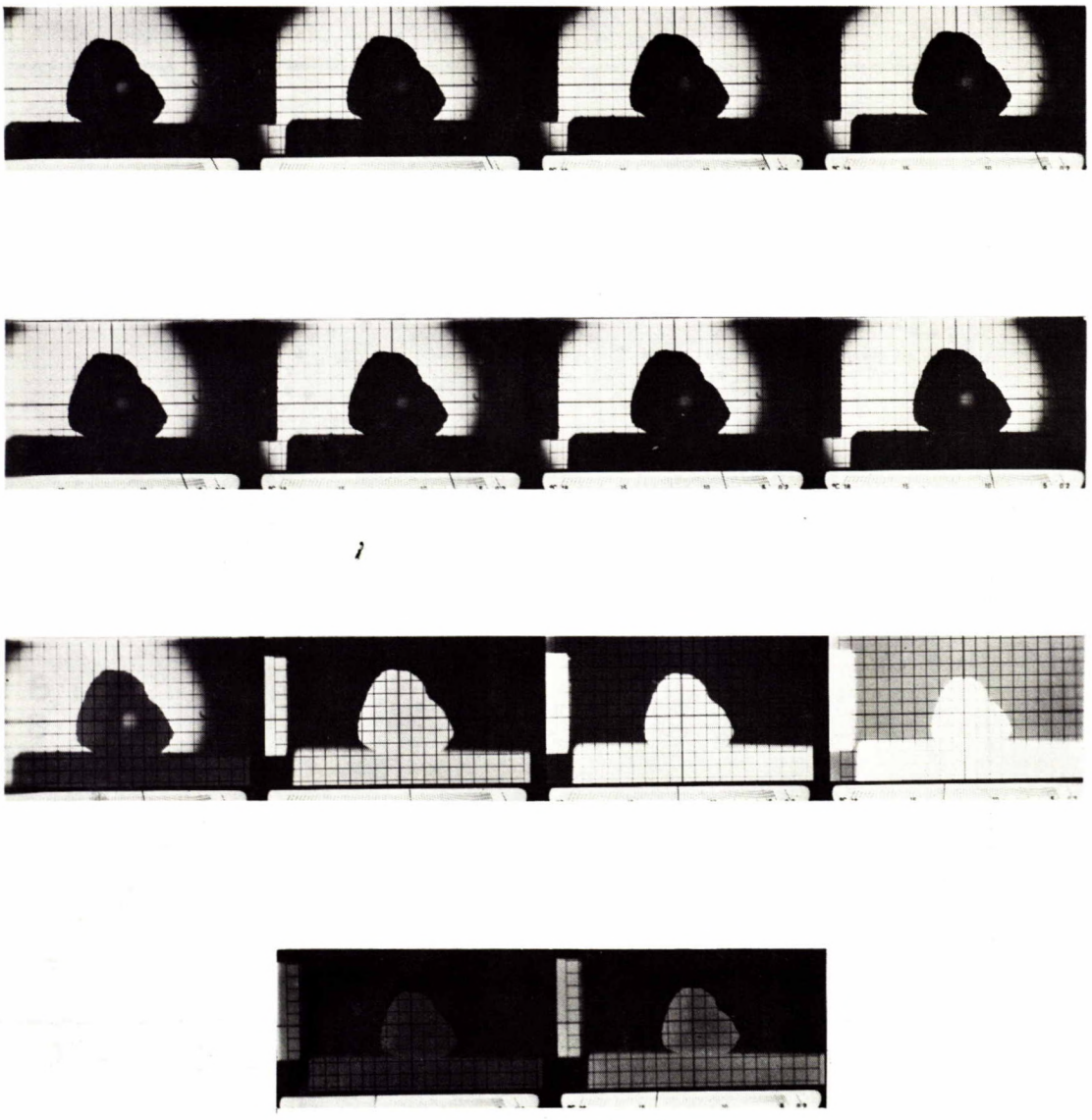

Figure 22. Sample of x = 1.7 material viewed in Leitz heating microscope during heating in a static air atmosphere to 1400°C.

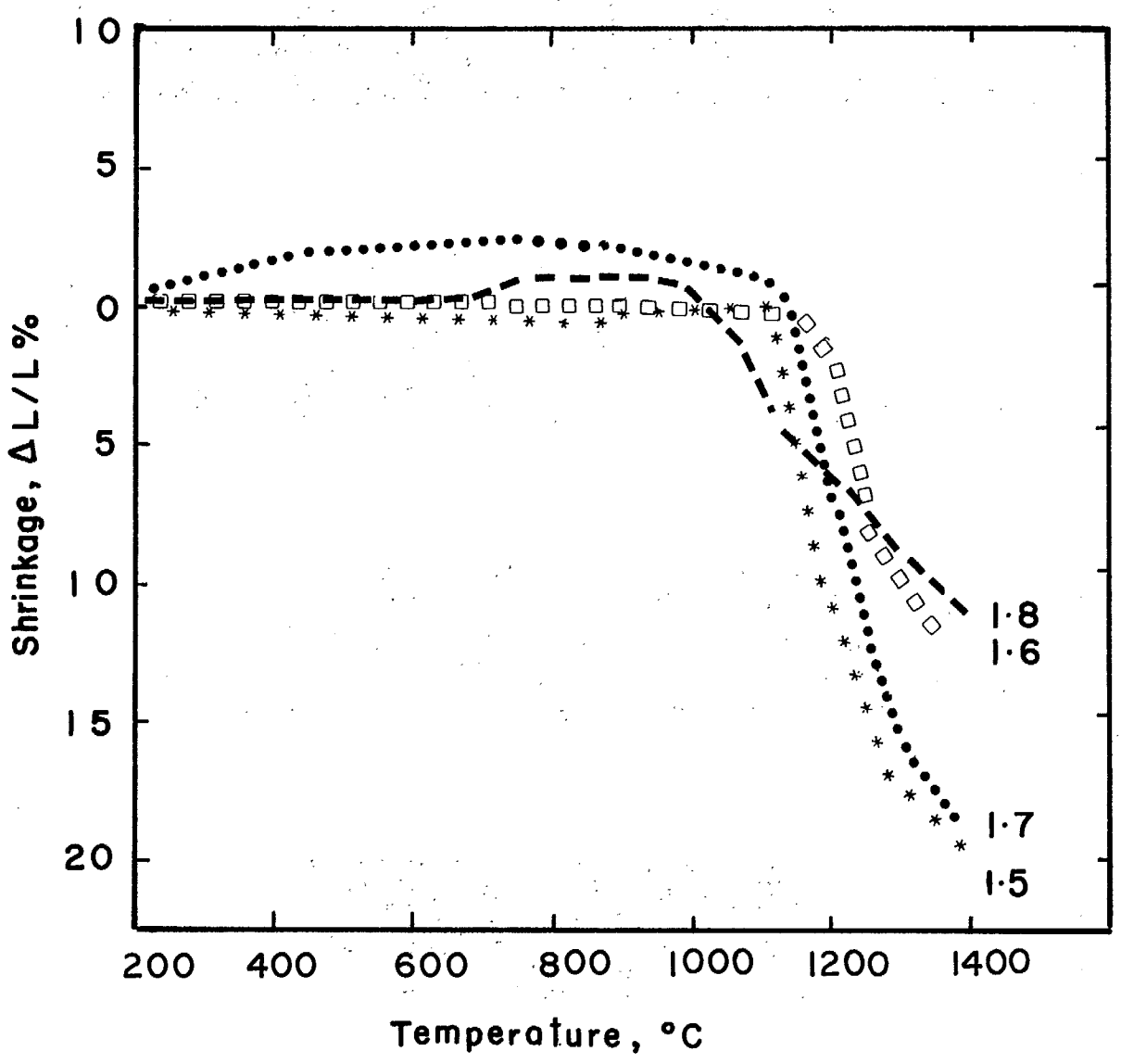

Figure 23. Typical sintering curves for the compositions shown on heating in a static air atmosphere.

The continuance of shrinkage at temperatures above 1300°C was significant. With increasing temperature, the vapour pressure of K_2O increases and the samples slowly become K-deficient. TGA shows a progressive increase in the rate of weight loss with increasing temperature above this point. As the material is of interest as a K-ion conductor, the development of surface deficient layers would undoubtedly introduce an unknown variable in determining the electrical characteristics of these materials. Consequently, all sintering of these materials was conducted at temperatures below 1300°C - the minor additional shrinkage that occurs above this temperature with a constant rate of heating was effectively maintained by incorporating a 3-hr soak period at the sintering temperature.

Subsequently, other samples having the composition $x = 1.8$, 1.7, 1.6 and 1.5 were heated in the microscope in a static air atmosphere and the melting point was determined. The results are presented in Figure 24. Although a liquidus and solidus line are given, this interpretation of the results may not be strictly correct. The solidus temperature was taken to be that at which the very fine projections from the sample surface first melted whereas the liquidus temperature was taken to be that at which the whole sample reached the hemispherical point. In practice, the small projections could well have a different composition from that of the bulk sample as they have a larger surface-to-volume ratio,

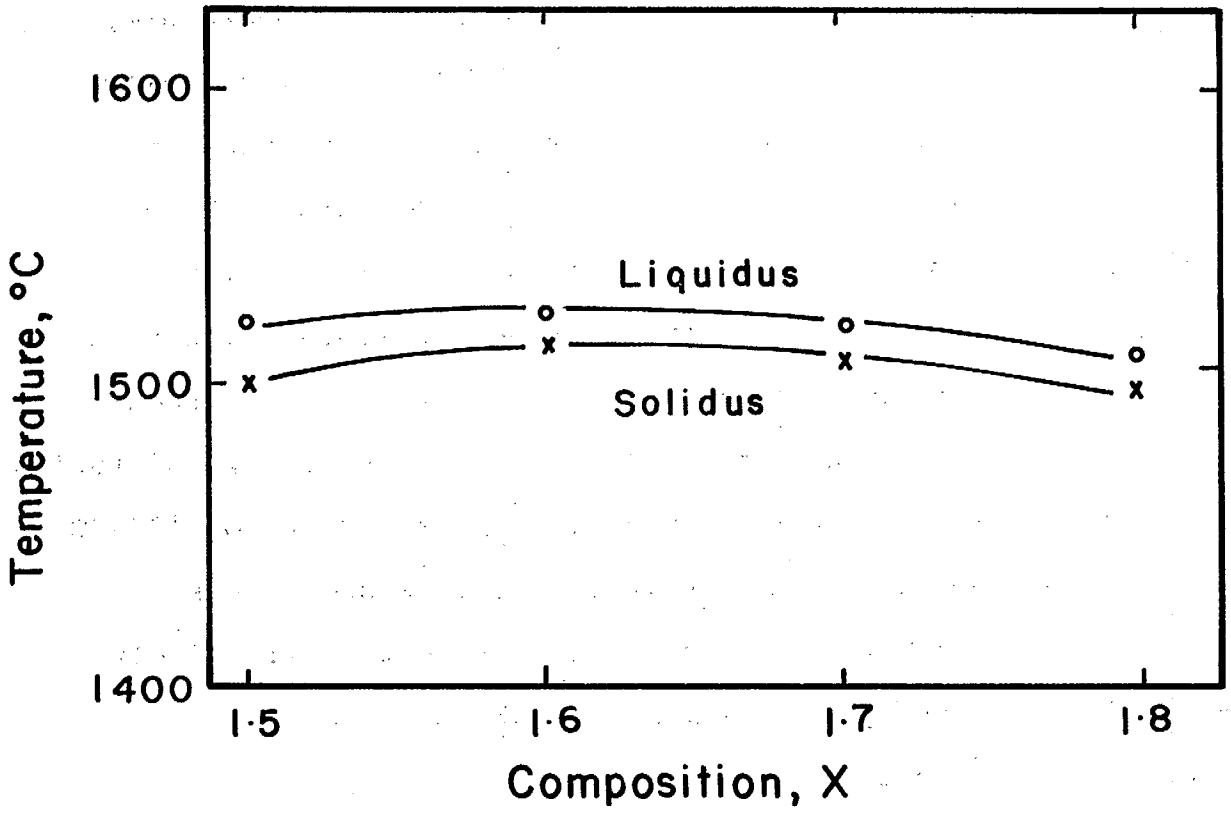

Figure 24. Variation of melting point of hollandite samples with composition.

facilitating the preferential loss of K_2O, and this could lead to the development of apparent solidus and liquidus temperatures for the $\bar{x}$ = 1.5, 1.6, 1.7 and 1.8 compositions that were shown by XRD to be single-phase materials. However, the results do show that the melting points of these compositions are relatively high and are also essentially independent of composition within this range.

As this project progressed, it became clear that the use of a PVA binder was unsuitable as it did not impart sufficient strength to the green-pressed samples. As a result, edges of the discs were commonly damaged and required excessive machining to obtain unblemished samples for characterizing the electrical and thermal properties. Consequently a commercially available polyvinyl acetate (Gelva V-7, available from Monsanto Canada Ltd., Toronto) together with a polyethylene glycol (Carbowax 400, available from Union Carbide Canada Ltd., Toronto) were used as a combined powder binder and powder lubricant respectively, as previous work had demonstrated that high-strength compacts could readily be obtained[15]. The technique for mixing these additives into the calcined powders was similar to that used for the initial PVA binder: each 100 g of powder was uniformly sprayed with a 200 mL solution of toluene containing 5 g Gelva V-7 and 2 g Carbowax 400. The powder was constantly mixed and turned on a polyethylene sheet during the spraying operation to ensure uniform distribution of the binder-lubricant system. The powder was allowed to dry for 1 hr prior to placing in an uncapped bottle and allowing to stand overnight prior to use. The resulting powder was free-flowing and possessed excellent pressing characteristics. Irrespective of composition, all green-pressed samples were much stronger than the bodies containing PVA; in addition, the pressed

density was also improved, Table 2. Although the use of such a high concentration of binder (5 wt %) and lubricant (2 wt %) in a raw material is normally avoided, it had been shown earlier that such a quantity was required with raw materials having a surface area of between 15 and 25 m^2/g [15]. Despite this concentration, no difficulty was experienced using the binder-burnout procedure employed with the powders containing PVA. As shown in Figure 21, DTA established that the burnout characteristics of the two binder systems were sufficiently similar to allow the same low-temperature heating schedule to be followed prior to firing.

As would be expected with any of the titanates which readily become non-stoichiometric on sintering, one of the more significant processing parameters in fabricating these materials was shown to be the atmosphere maintained (or developed) in the furnace during the sintering stage.

Effect of Furnace Atmosphere on Sintered Product

After the binder-burnout stage, the samples were heated at 200°C/hr in either an oxidizing or reducing atmosphere at the sintering temperature of 1250°C and maintained at that temperature for 3 hr. Thereafter, the furnace and samples were allowed to cool naturally and the samples were removed from the furnace at any temperature less than 750°C. These sintering conditions were arbitarily chosen as a compromise

TABLE 2

Green Bulk Densities of Materials Containing Gelva V-7 Binder and Carbowax 400 Lubricant

Composition	Diameter cm	Thickness cm	Weight g	Density g/cc	Average Density* g/cc
1.5	3.322	1.125	20.7176	2.09	
	3.343	1.095	20.3667	2.12	
	3.348	1.054	19.6782	2.12	2.11
	3.353	0.358	6.7444	2.13	
	3.348	0.318	5.9773	2.14	
	3.345	0.348	6.5774	2.15	2.14
1.6	3.226	1.173	20.1782	2.10	
	3.239	1.158	19.9469	2.09	
	3.233	1.161	20.1257	2.11	2.10
	3.259	0.414	7.2147	2.09	
	3.272	0.411	7.2214	2.09	
	3.307	0.383	6.9647	2.04	2.07
1.7	3.309	1.097	20.2582	2.15	
	3.315	1.097	20.2026	2.13	
	3.312	1.100	20.1566	2.13	2.14
	3.312	0.381	7.1137	2.17	
	3.317	0.450	8.1972	2.15	
	3.317	0.396	7.3443	2.14	2.15
1.8	3.556	0.983	22.1453	2.27	
	3.541	0.988	22.1139	2.27	
	3.546	0.998	22.3443	2.27	2.27
	3.597	0.318	7.1654	2.22	
	3.597	0.318	7.1290	2.21	
	3.586	0.320	7.1808	2.22	2.22

All samples were uniaxially pressed at 35 MPa in order to form the compact and were finally isostatically pressed at 280 MPa.

* Precision of the density data is $\pm$0.01g/cc.

between the high temperature (1400°C) needed to complete the shrinkage of these materials as shown by the hot-stage microscope and the lower temperature (less than 1300°C) required to avoid the significant loss of K_2O by volatilization as shown by the TGA data. The use of a lower temperature and longer sintering time than was employed in the heating microscope would also lead to a slower migration of grain boundaries and hence probably to less trapping of micropores within the individual grains, a phenomenon that is characteristic of sintering reactive materials too rapidly.

Sintering in Air

The initial firings were conducted using an air atmosphere. Because of the known tendency of titanates to be readily reduced, coupled with the observed appearance of a grey core in the samples heated in a static air atmosphere in the heating microscope, it was decided to use a slowly flowing atmosphere in the furnace in an attempt to maintain oxidizing conditions. However, it was found that the colour of the samples, which is a sensitive indicator of the state of oxidation, varied slightly and progressively from cream for $x = 1.8$ material to grey for the $x = 1.5$. Because of this variation and its probable effect on the thermal, electrical and possibly microstructural properties of these materials, it was clear that fully oxidizing conditions should be used during firing to consistently sinter these materials. Consequently, many of the subsequent firings were conducted using oxygen.

Sintering in Oxygen

Because of the minor grey colour of the air-fired samples, it was assumed that all the materials would be readily sintered in a fully oxidized state (cream colour) in oxygen. In general, this is true, although the manner in which the firing is conducted is crucial. Variables such as the flow rate, sample size, and placement of the various sample compositions with respect to the direction of oxygen flow were found to have a marked influence of the oxidation state of the sintered materials. For example, several times the more TiO_2-rich compositions, $x = 1.6$ and 1.5, were sintered in a reduced state in a continuously flowing pure oxygen atmosphere.

Initially, the thinner discs were used to examine the firing parameters that control the state of oxidation as they used only one third the amount of material required for the thicker cylinders. Table 3 indicates the results of the initial firings.

TABLE 3

Effect of Firing Conditions on the Colour of Sintered Material

Dry O_2	85 L/hr	1.5(G)		1.6(G)	1.7(C)	1.8(C)
Dry O_2	285 L/hr	1.5(C)*		1.6(C)	1.7(C)	1.8(C)
Wet O_2	85 L/hr	1.5(C)	1.4(G)	1.6(C)	1.7(C)	1.8(C)

*Sample badly warped and cracked.

Direction of gas flow was from left to right using Industrial grade O_2 from Liquid Carbonic Canada Ltd., which was either as-received (dry) or first bubbled through water at room temperature (wet). The sample colour is given in parentheses as either cream, (C), or grey, (G).

From these results, several conclusions may be drawn:

- the TiO_2-rich compositions- x = 1.4, 1.5 and 1.6, cannot be oxidized in a low flow rate of dry oxygen,
- as the TiO_2 content is reduced so is the material more readily oxidized,
- an increase in the flow rate will eventually oxidize all samples but at the expense of cracking the first disc due to thermal gradients across the disc induced in the incoming cold gas,
- wet oxygen is a more effective oxidant than dry gas.

However, in a subsequent experiment, a sample of x = 1.6 material was sintered in oxygen flowing at a rate of $\simeq$285 L/hr using a sacrificial baffle disc between the sample and the incoming gas to avoid thermal gradients and cracking (conditions that would be expected to produce a cream, fully oxidized product, Table 3); the sample was grey. From these and other experiments it became clear that there was a synergistic effect operating in which both the oxygen flow rate and its water content were critical to fully oxidizing these materials.

This combined effect of flow rate and water content was not immediately apparent in this work. The initial firings were carried out using the dry gas and a flow rate of 85 L/hr. The second firing used wet oxygen in an attempt to determine the effect of gas composition on the fired density. In both cases, all the compositions were cream after firing and there was

no difference in the sintered density of the samples as a result of increasing the water content of the sintering atmosphere. Consequently, it was assumed that a wet atmosphere was unimportant in sintering these materials. However, as more samples were sintered, this assumption had to be questioned as some of the TiO_2-rich compositions sintered to a grey colour. Subsequently, it was shown that the colour depended not only on composition under a given set of firing conditions but also on the sample size and the number of samples sintered at any one time. For example, in one sintering, three samples of 1.6 material were fired in wet oxygen with a flow rate of 85 L/hr. Each sample was identical to its neighbour as far as initial composition was concerned yet the first two samples, with respect to the direction of gas flow, were cream while the last sample was grey. A subsequent firing of a similar disc formed from the same batch of powder gave a cream product. However, the grey colouration returned in similar subsequent firings in which only one sample was fired but in a dry atmosphere. The difference in colour of 1.6 material in which the only variable was the moisture of the gas is shown in Figure 25.

Because of these results it is difficult to define the conditions that give either the cream or grey colour for each composition for, in cases where both colours are produced in the same firing, the result appears to depend on the local atmosphere around each sample and that can be clearly different from that of the incoming gas. An additional variable that

probably had a considerable influence on the early results was the water content of the oxygen gas as supplied by the producer. It is probable that what was regarded as a 'dry' gas and used in the first two firings to examine the effect of adding moisture to the oxygen was, in fact, wet enough to produce fully oxidized samples and as a result there was no difference between the dry and wet firings initially. Unfortunately, the moisture content of that particular cylinder of oxygen was not known and hence the reason for the first firings being completely successful remains speculative.

Although not intended as a definitive statement of the firing conditions, Appendix B gives an indication of the limits in which both grey and cream samples were produced in this work.

It would be expected that the density of these samples, which were much greater than those from which the data presented in Figures 19 and 20 were taken, would be slightly lower because of the increased die-wall friction effects developed by the thicker discs during the initial forming stage and also the greater density gradients developed in the larger samples as a result of internal powder friction developed during the isostatic-pressing process. The results, presented in Table 4, confirm this trend to a lower sintered density with larger samples.

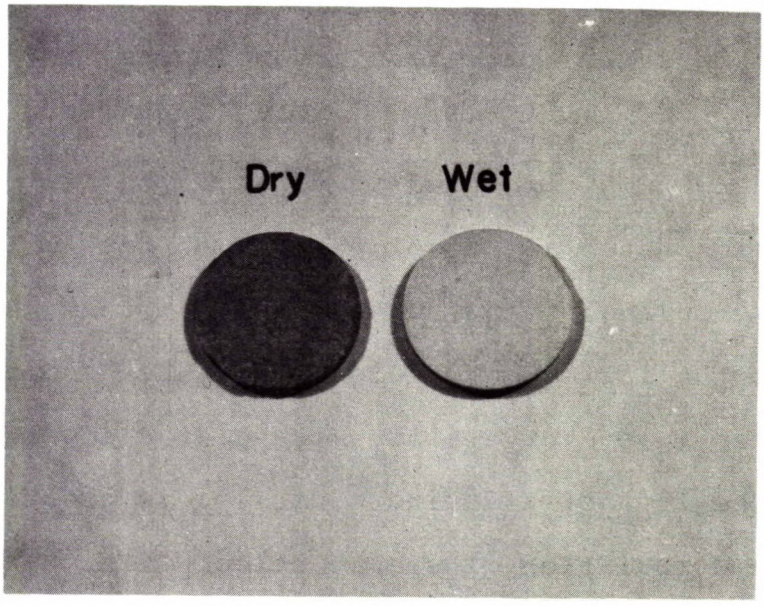

Figure 25. Samples of x = 1.6 material sintered at 200°C/hr to 1250°C and maintained at that temperature for 3 hr in an oxygen atmosphere. Samples approximately 2.7 cm in diameter.

It can also be seen that the density of the sintered discs is independent of the colour developed by the product. In several cases, samples that had been fired initially in a dry atmosphere under conditions which produce a grey disc and had subsequently been refired to the same temperature for the same time in a wet atmosphere and converted to a cream colour showed no change in bulk density. In contrast to the ball milled materials discussed in pages 13 to 24, none of the freeze-dried materials developed any surface whiskers of a K-rich phase during firing, suggesting that the greater reactivity of the latter materials allows the K component to be incorporated into a crystalline phase at a lower temperature and thereby the loss of K during sintering is greatly reduced.

The correlation of sample colour with oxidation state of these materials was suggested by the results obtained on sintering in a reducing atmosphere - in all cases, a completely black product was obtained.

Sintering in Hydrogen

Samples sintered in a reducing atmosphere were initially heated in an oxidizing atmosphere up to 400°C following the procedure given above to remove the binder and lubricant from the compacts prior to sintering.

TABLE 4

Fired Bulk Densities of Materials Containing Gelva V-7 Binder and Carbowax 400 Lubricant

Composition	Diameter cm	Thickness cm	Weight g	Density g/cc	Average density g/cc	Colour
1.5	1.145	0.311	18.7982	3.58		c
	1.148	0.314	18.9398	3.56		c
	1.148	0.314	18.8496	3.54	3.56	c
	1.121	0.103	5.6037	3.60		g
1.6	2.675	0.973	18.8754	3.45		g
	2.680	0.955	18.6563	3.46		g
	2.677	0.953	18.7654	3.50	3.47	g
	2.695	0.338	6.7412	3.50		g
	2.705	0.333	6.7383	3.52		c
	2.733	0.309	6.4897	3.57	3.53	c
1.7	2.766	0.902	18.8750	3.48		c
	2.768	0.902	18.8322	3.47		c
	2.758	0.906	18.7831	3.47	3.47	c
	2.781	0.318	6.6372	3.44		c
	2.771	0.361	7.6535	3.52		c
	2.774	0.325	6.8555	3.49	3.48	c
1.8	2.997	0.831	20.8362	3.54		c
	3.020	0.826	20.8572	3.53		c
	3.015	0.843	21.0517	3.50	3.52	c
	3.035	0.264	6.6892	3.50		c
	3.025	0.267	6.7371	3.51		c
	3.043	0.267	6.7223	3.47	3.49	c

c = cream colour
g = grey colour

Thereafter, the samples were heated in a mixture of 95% N_2 - 5% H_2 using a flow rate of 85 L/hr . In all cases, the gas was used as received; it was neither humidified nor dried prior to introduction into the furnace. Figure 26 shows the difference in appearance between samples fired to 1250°C with a 3-hr soak using either an oxidizing or reducing atmosphere. The figure demonstrates that, irrespective of the atmosphere, the diametral shrinkage can be correlated with composition: the lower the K and Mg content, the higher the shrinkage.

One of the more unusual features of the H_2-fired samples was the gradual development of a white efflorescence on the surface of each sample. This effect only occurred on those discs that were exposed to the atmosphere; samples stored over a silica gel dessicant were stable with time. Figure 27 compares the appearance of discs immediately after firing with similar samples that had been exposed to the atmosphere for a period of 14 days. Although the efflorescence is most clearly visible on the $x = 1.5$ material it is also present to a lesser extent on the $x = 1.6$ and 1.7 samples. After approximately one month, all samples become coated to the same extent.

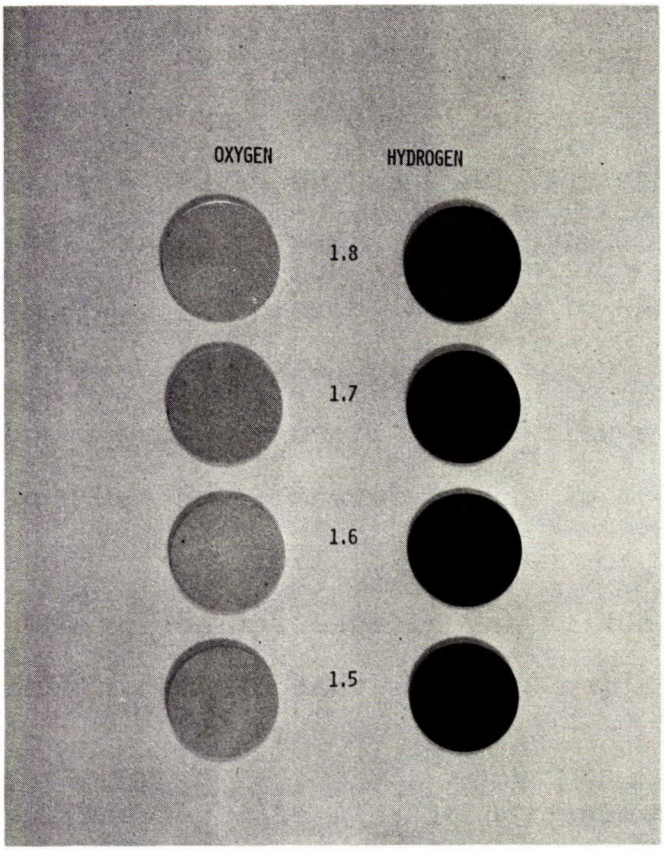

Figure 26. Comparison of sintered discs of each composition after firing in oxidizing and reducing conditions.

An optical examination of this material showed that it was formed with a dendritic habit and that it was not uniformly distributed over the surface of the disc. As shown in Figure 28, the areas between the dendrites do contain additional efflorescence but at a much lower concentration. It is probable that this is the result of a surface diffusion mechanism that allows well-developed dendrites to be formed at the expense of material originally present in the nearly clear zones. Under crossed polars, it can be seen that the dendrites are well crystallized and birefringent. There is no evidence of any preferred orientation of the dendrites with respect to the individual grains in the surface of the disc. The lack of any diffuse reflection from the areas of low concentration suggests that the material in this part is amorphous.

Examination of this efflorescence using a scanning electron microscope (SEM) confirmed the uneven distribution of this phase but failed to reveal the presence of any dendritic material. This was presumably due to the different environment inside the sample chamber of the SEM at a vacuum of 1.33×10^{-2} to 1.33×10^{-3} Pa, compared with the normal atmosphere to which the samples were exposed during the optical examination. It had been noted that the form of this phase was very sensitive to humidity, the microstructure shown in Figure 28(a) being completely destroyed within one second by breathing gently on the surface of the disc. Hence, it was

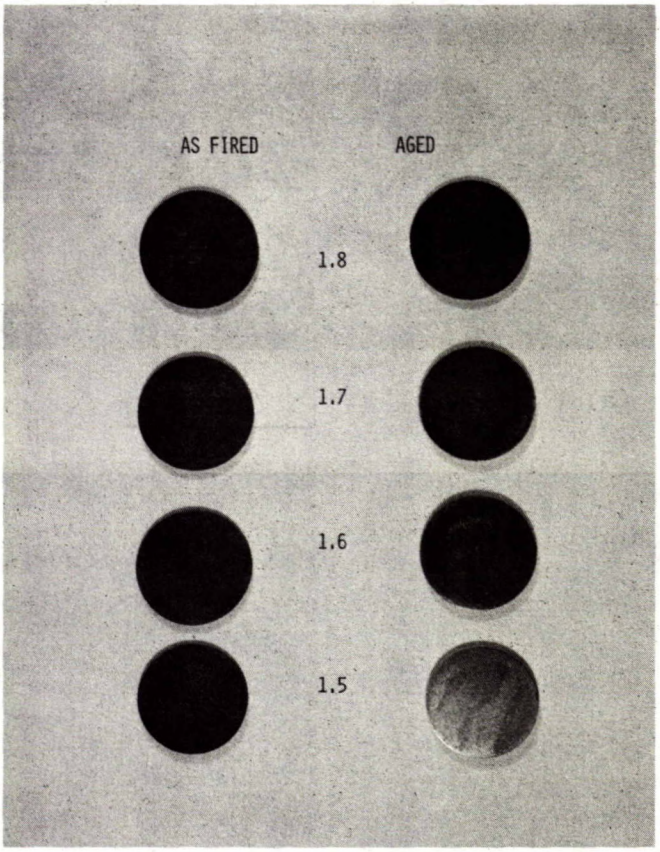

Figure 27. Comparison of as-fired samples with similar material after exposure to the atmosphere for 14 days. Samples fired in dry 95%N_2-5%H_2 atmosphere to 1250°C for 3 hr.

(a) 500 μm

(b) 500 μm

Figure 28. Development of efflorescence on the surface of x = 1.8 material after firing in a reducing atmosphere and exposing to a humid atmosphere for one month

(a) Reflected light, normal illumination
(b) Reflected light, crossed polars.

assumed that a deliquescent, hydrated crystalline phase had been produced. Under the vacuum of an SEM, the hydrate would rapidly decompose and the dendritic morphology would be lost. It is for this reason that the SEM micrograph shown in Figure 29 fails to show any characteristic crystal habit of the efflorescent phase.

From a cursory examination of the surface of the sample for the concentration distribution of the components, i.e., K, Mg and Ti, it appeared that the efflorescence had a higher concentration of K and a lower concentration of Ti than the disc itself, as shown in Figure 30. However, because of the low density of the efflorescence, there was no clear delineation between the superficial phase and the substrate. Consequently, the X-ray emission spectrum was obtained for both the general area shown in Figure 30 and for the circular feature shown in the centre of the micrograph. The results are shown in Figure 31 and confirm the very high concentration of potassium in the efflorescence. It is most probable that the low concentration of titanium indicated at point A in Figure 31 originates from the substrate, it being impossible to ensure that the primary beam of the SEM excites only the surface deposit and does not penetrate to the sample surface. Consequently, it is assumed that the efflorescence is composed entirely of a potassium-containing phase.

The other ions that may be present in the efflorescence would have an atomic number below 11 (Na) which is the lower limit of the Kevex energy-dispersive spectrometer used in

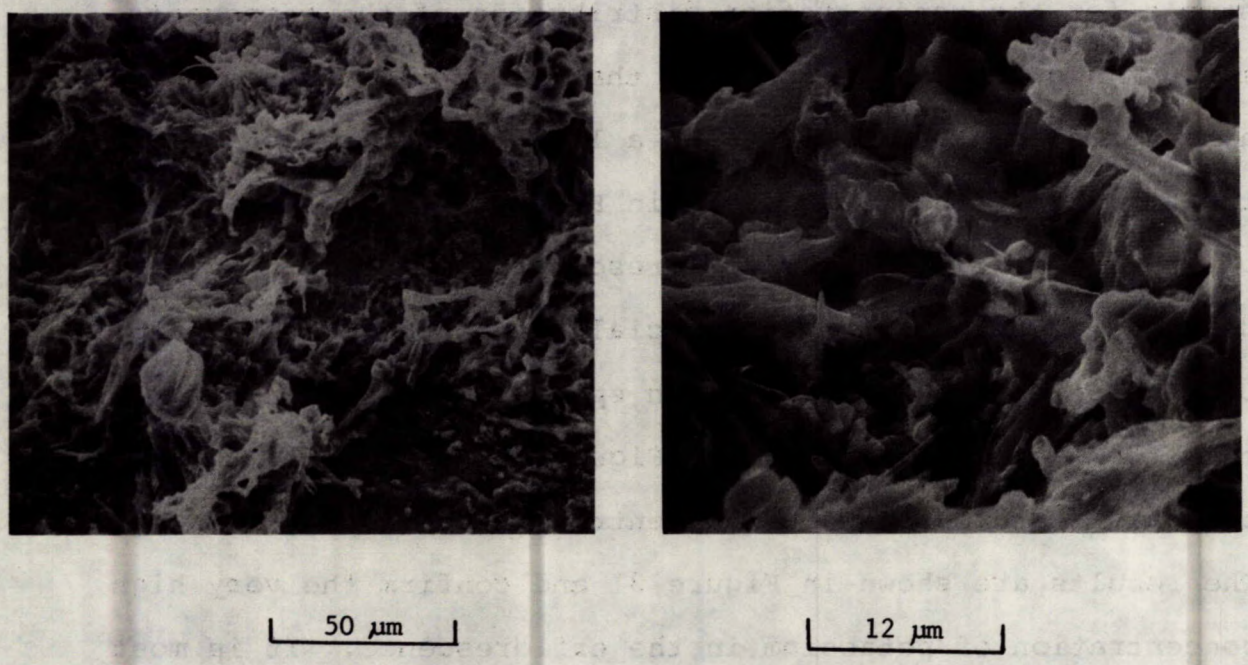

Figure 29. SEM micrographs of the surface of x = 1.8 material fired under reducing conditions and exposed to the atmosphere for 14 days.

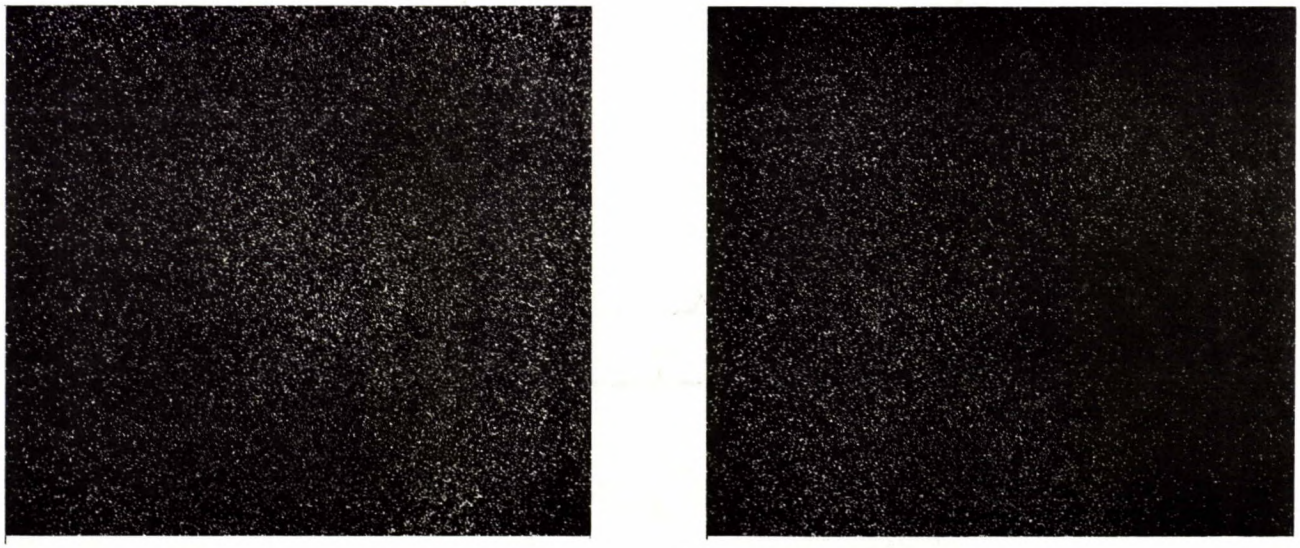

K Ti

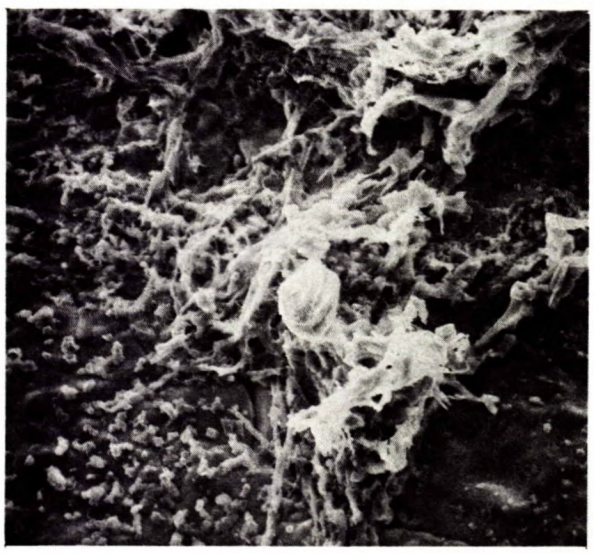

50 μm

Figure 30. Comparison of the elemental distribution of potassium and titanium with the distribution of the efflorescence on the surface of x = 1.8 material.

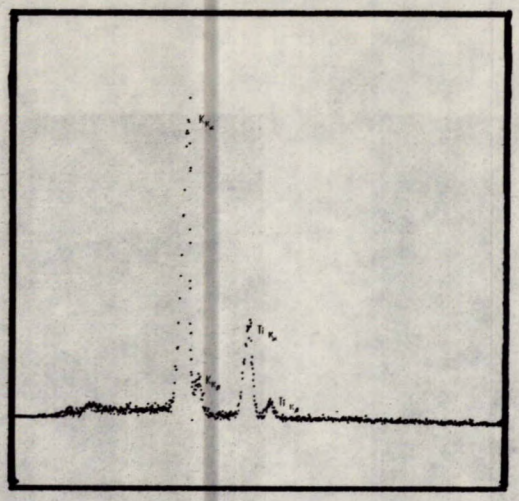

Total area

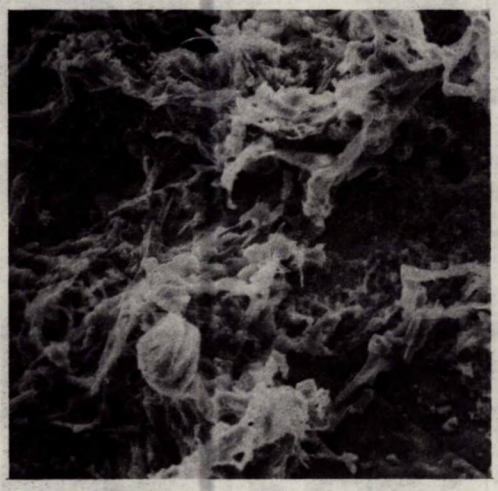

x 500

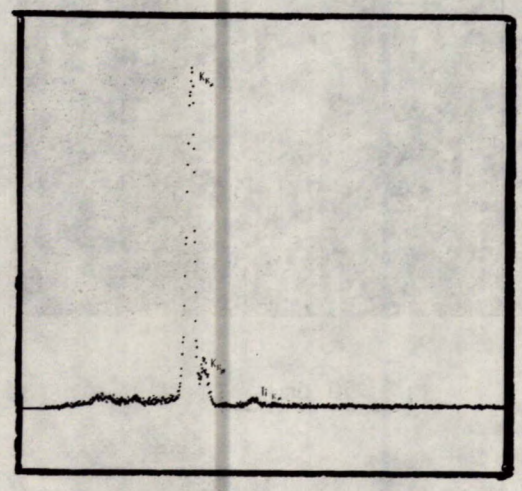

Point A

Figure 31. X-ray emission spectra of the surface of x = 1.8 material, after firing and exposing to the atmosphere for 14 days, showing the high concentration of potassium in the efflorescence.

conjunction with a Cambridge Instruments Stereoscan Mark IIA SEM to examine these samples. From this point of view, it is possible that any or all of the following elements could be present: H, He, Li, Be, B, C, N, O, F, and Ne. However, as the deposit is only formed under humid conditions, it is most probable that an oxide hydrate or hydroxide is formed initially and, with time, this may react with atmospheric CO_2 to form a normal or basic carbonate or bicarbonate. The virtually instantaneous evolution of gas from a sample of the efflorescence when treated with 10% HCl solutions suggests the presence of a carbonate or bicarbonate.

Unfortunately, it was not possible to obtain a complete identification of this phase using X-ray powder diffraction techniques as the pattern was complex, suggesting the presence of more than one phase. However, the data in Table 5 indicates that $KHCO_3$ is present together with other unidentified phases. Hence, it was concluded that, under reducing conditions, a potassium oxide is formed as a separate phase and this slowly reacts with moisture in the atmosphere to form KOH which gradually reacts with atmospheric CO_2 to form $KHCO_3$ and other hydrated carbonates or bicarbonates.

Because of the considerable difference in the stability of the oxidized and reduced materials to a humid atmosphere at ambient temperatures, a detailed examination of the microstructure of each composition fired in both O_2 and H_2 was made using both optical and SEM techniques. This also provided confirmation of the superiority of the wet-chemical

TABLE 5

Comparison of the 'd' Values Obtained from an X-Ray Powder Diffraction Pattern of the Efflorescence with those for Potassium Bicarbonate

Efflorescence		Potassium Bicarbonate	
d Å*	I	d Å*	I
7.8	m		
7.0	m	7.0	m
		5.5	w
4.2	m	4.2	w
3.8	w	3.75	s
3.6	w		
3.2	w	3.18	w
2.95	s	3.00	s
2.80	s	2.80	s
2.65	w		
		2.60	s
2.50	m		
2.37	s	2.40	m
		2.30	m
2.20	w	2.26	m
2.10	w		
2.02	w	2.02	m
1.86	m	1.85	m
		1.80	m
		1.75	m
1.69	w		
1.61	m		
		1.53	w
		1.46	w
1.34	w	1.32	m

s - strong,

m - medium, and

w - weak

* - 1 Å ≡ 10 nm

process to provide homogeneous microstructures in contrast to the heterogeneous materials developed by the conventional ball milling process discussed in Part I of this report.

Microstructure of Fired Materials

Optical Microscopy

Samples were mounted and polished using a technique described elsewhere[19] and subsequently examined in reflected light using partially crossed polars to reveal the grain size and the micro- and macro-porosity. Typical results obtained in this manner are shown in Figures 32 to 40.

It can be seen that there is a considerable difference between the microstructure of ball milled materials shown in Figures 4 to 7 and that of the freeze-dried powders. Admittedly, there are several differences in processing conditions between the two sets of materials, such as sintering atmosphere, temperature of sintering and soak time that give rise to the much finer grain size of the ball milled products. However, the most significant is probably the sintering temperature. Comparison of Figures 32(a) and 32(b) illustrates this effect well. The very fine-grained microstructure of 32(a) is thought to result from the cooling effect of the high flow rate of oxygen required to maintain a cream coloured sample (285 L/hr) compared with the very coarse-grained material shown in 32(b) which was fired to apparently the same temperature but using a slower flow rate of gas at 85 L/hr. Even in Figure 32(b), there are areas of fine-grained material suggesting that these materials

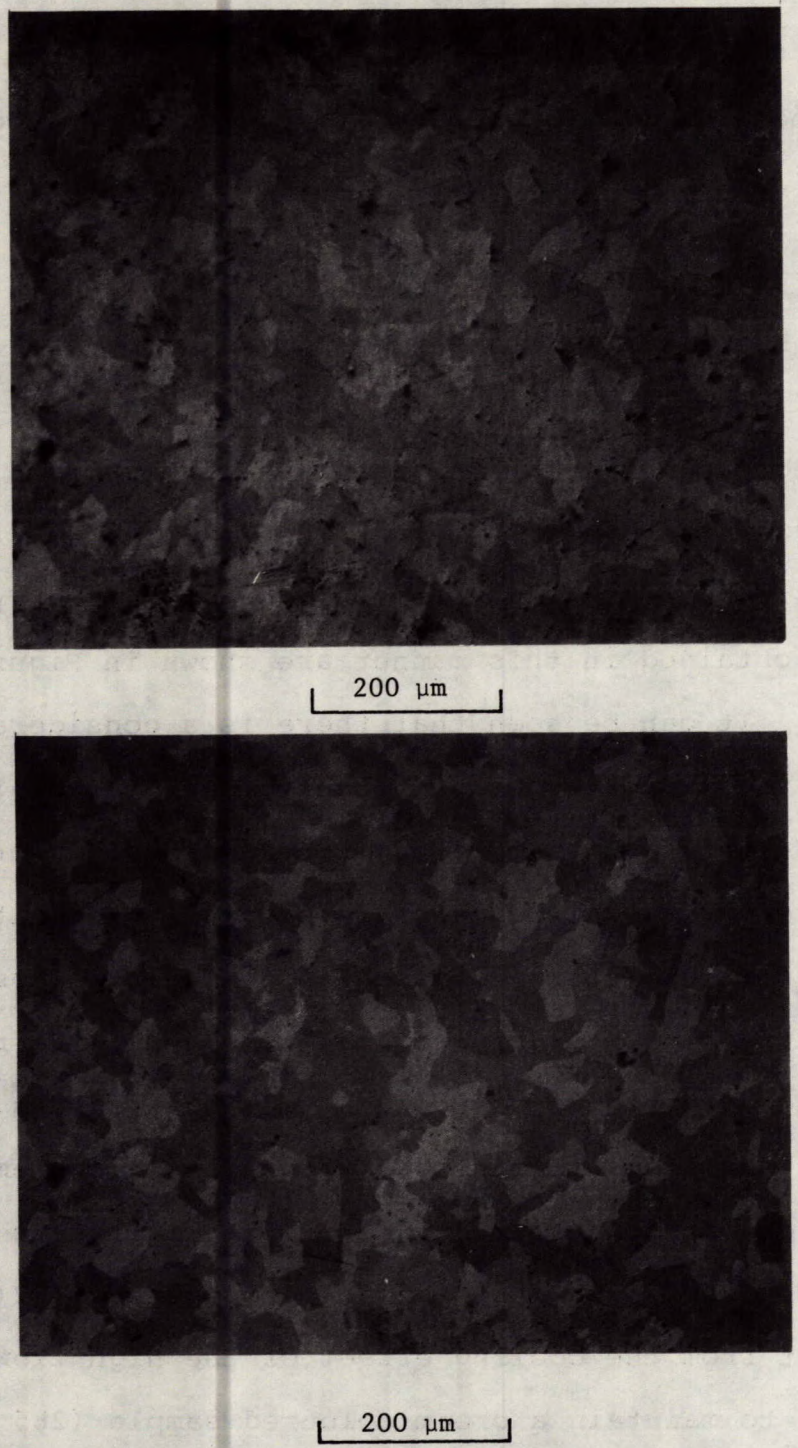

Figure 32. Microstructure developed in x = 1.6 material after firing at 200 °C/hr and holding at that temperature for 3 hr

(a) sintered in dry oxygen at a flow rate of 285 L/hr.
(b) sintered in dry oxygen at a flow rate of 85 L/hr.

(a) 200 μm

(b) 200 μm

Figure 33. Microstructure developed in x = 1.5 material after firing at 200°C/hr to 1250°C and holding at that temperature for 3 hr

(a) Sintered in a dry oxygen atmosphere.
(b) Sintered in a wet oxygen atmosphere.

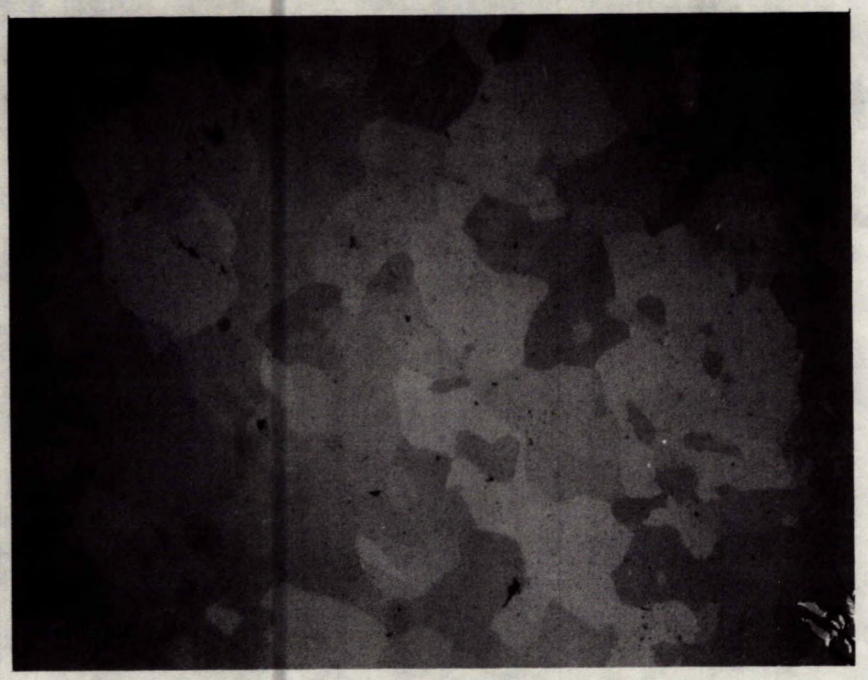

(a) 200 μm

(b) 200 μm

Figure 34. Microstructure developed in x = 1.6 material after firing at 200°C/hr to 1250°C and holding at that temperature for 3 hr

(a) Sintered in a dry oxygen atmosphere.
(b) Sintered in a wet oxygen atmosphere.

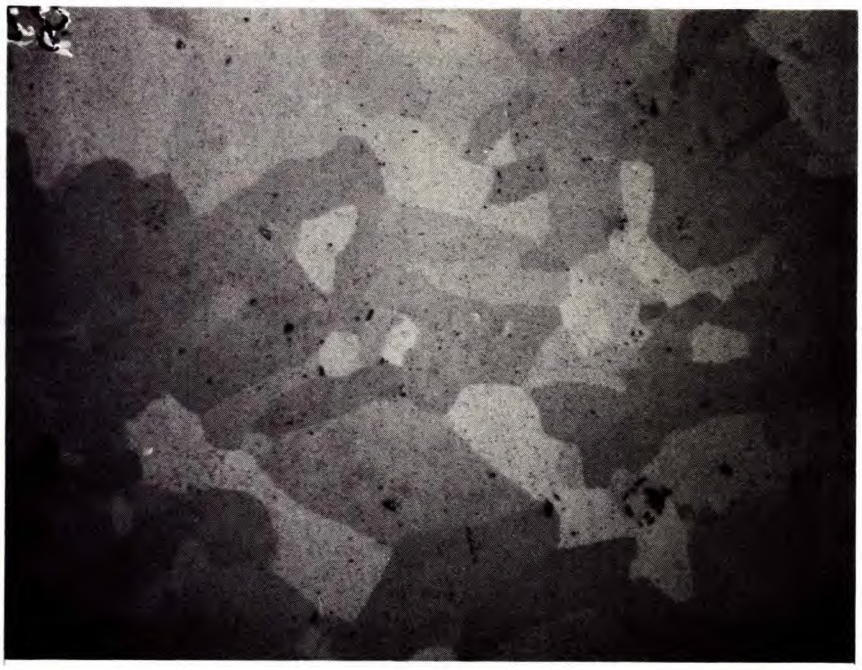

(a) 200 μm

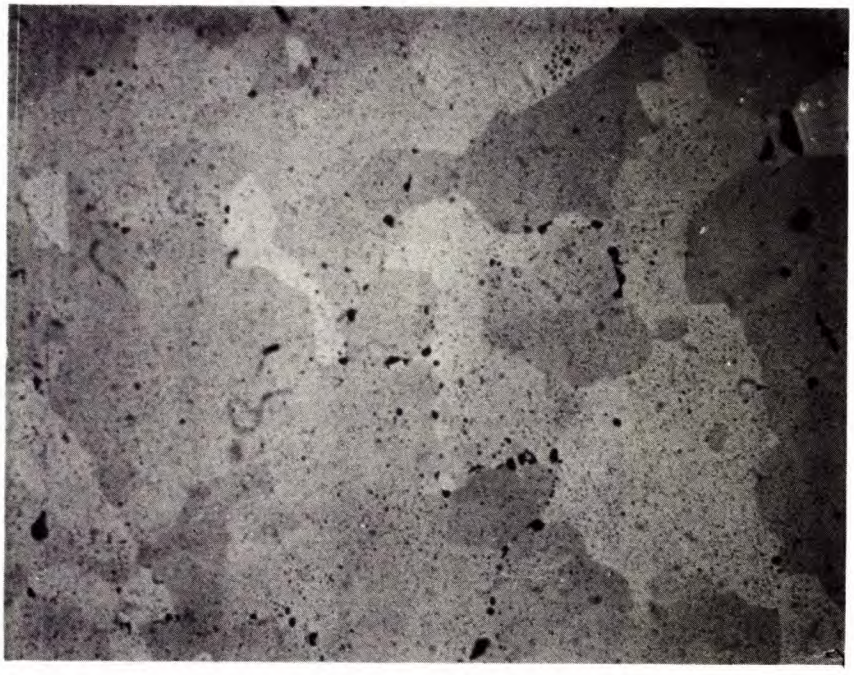

(b) 200 μm

Figure 35. Microstructure developed in x = 1.7 material after firing at 200°C/hr to 1250°C and holding at that temperature for 3 hr

(a) Sintered in a dry oxygen temperature
(b) Sintered in a wet oxygen temperature

(a) 200 μm

(b) 200 μm

Figure 36. Microstructure developed by x = 1.8 material after firing at 200°C/hr to 1250°C and holding at that temperature for 3 hr

(a) Sintered in a dry oxygen atmosphere
(b) Sintered in a wet oxygen atmosphere.

(a) 200 μm

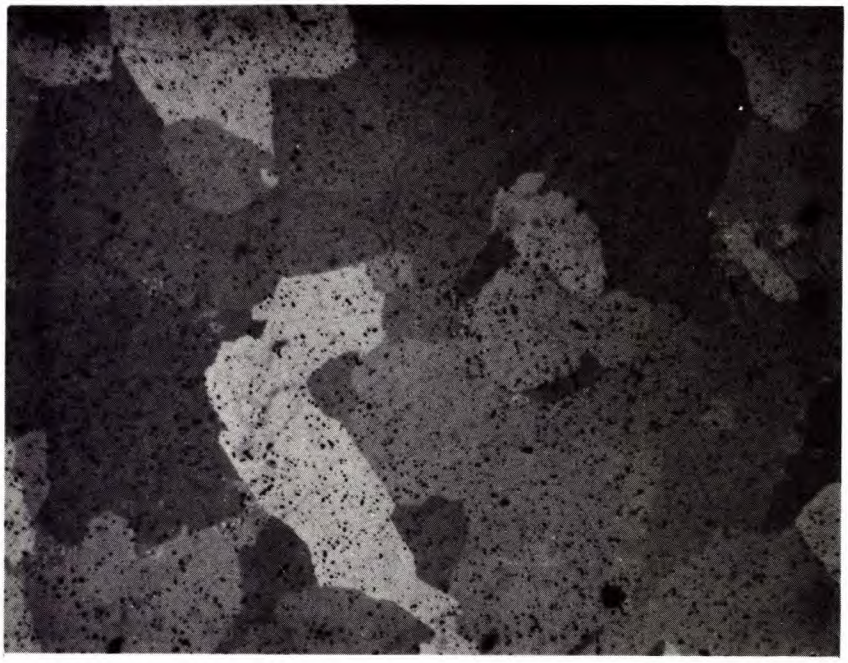

(b) 200 μm

Figure 37. Microstructure developed by x = 1.5 material after firing at 200°C/hr to 1250°C and holding at that temperature for 3 hr

(a) Sintered in a dry 5% H_2-95% N_2 atmosphere
(b) Sintered in a wet 5% H_2-95% N_2 atmosphere

(a) 200 μm

(b) 200 μm

Figure 38. Microstructure developed by x = 1.6 material after firing at 200°C/hr to 1250°C and holding at that temperature for 3 hr

(a) Sintered in a dry 5% H_2-95% N_2 atmosphere
(b) Sintered in a wet 5% H_2-95% N_2 atmosphere.

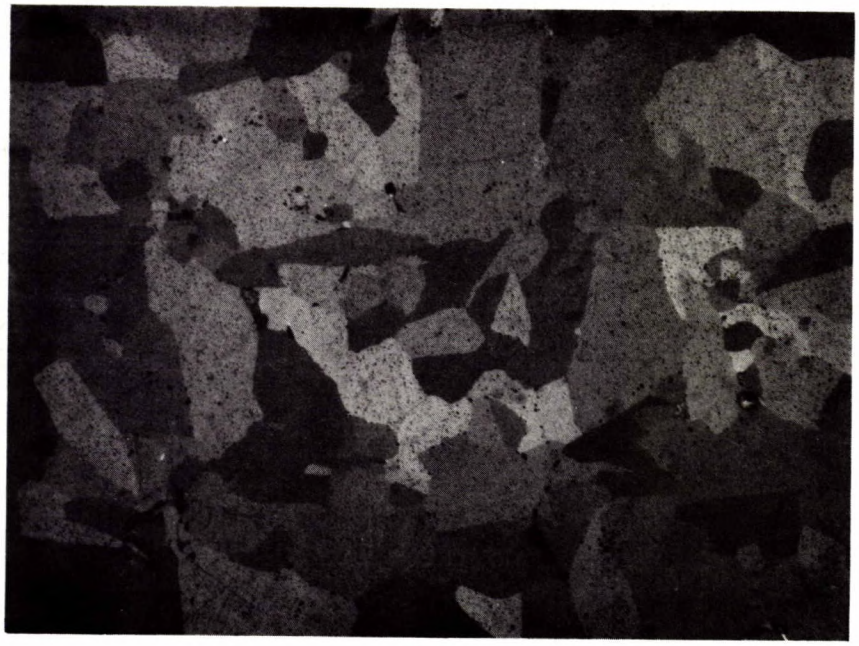

(a) 200 μm

(b) 200 μm

Figure 39. Microstructure developed in x = 1.7 material after firing at 200°C/hr to 1250°C and holding at that temperature for 3 hr

(a) Sintered in a dry 5% H_2-95% N_2 atmosphere
(b) Sintered in a wet 5% H_2-95% N_2 atmosphere.

(a) 200 μm

(b) 200 μm

Figure 40. Microstructure developed in x = 1.8 material after firing at 200°C/hr to 1250°C and holding at that temperature for 3 hr

(a) Sintered in a dry 5% H_2-95% N_2 atmosphere
(b) Sintered in a wet 5% H_2-95% N_2 atmosphere.

undergo a very rapid grain growth between 1200°C and 1250°C.

Comparison of Figures 33 to 40 shows that as the concentration of K and Mg increases, i.e., as x increases, the average grain size decreases. However, although a strong dependence of grain size on moisture content of the sintering atmosphere would be expected for the non-stoichiometric oxide systems, this is not found in the present materials to any great extent. The grain size is essentially unchanged on increasing the moisture content of either an oxidizing or reducing atmosphere. This result is in disagreement with the data reported for the behaviour of TiO_2 in various atmospheres[20] in which it was shown that the presence of steam significantly increased the crystallite size developed on heating powdered samples.

It has also been indicated that the grain size of TiO_2 is increased by firing in a reducing atmosphere[20]. However, this was not found to be the case in the present materials. All compositions examined tended to develop a smaller grain size in a hydrogen-containing atmosphere than in oxygen, although the difference in grain size between the two atmospheres is very small.

Despite the care taken to produce relatively high green-density materials prior to pressing, all the materials continued to retain isolated areas of macroporsity approximately 10 to 20 μm in diameter. These pores result from particle bridging occurring during the fabrication stages despite a lubricant being added to the material prior to pressing.

In addition, all the samples fired under the different sintering conditions retained a fine well-dispersed microporosity. During the initial stages of sintering at approximately 1200°C these micropores were situated at the grain boundaries of a relatively fine-grained material - a typical example of which is shown in the centre of Figure 32(b). With the further increase of 50°C to the final sintering temperature, a very rapid grain growth occurs in which the grain size increases approximately one order of magnitude. At this point, the grain boundaries are moving too rapidly to be pinned by the pores. Consequently, the boundaries sweep through many pores and thus relatively large crystals containing numerous micropores are developed. Once the pores become isolated, they can no longer be eliminated by a vacancy diffusion mechanism in which a grain boundary acts as a vacancy sink. The only way these micropores can be eliminated is by using a much slower sintering rate, by either sintering at a lower temperature or by using a lower heating rate (or both), so that the rate of grain boundary migration is greatly reduced and the pores can be eliminated gradually as they are intercepted by the boundaries.

One of the surprising aspects of the microstructures of hydrogen-fired materials is the lack of any evidence of a second phase that must be present for such an extensive amount of efflorescent material to be formed on exposure to a humid atmosphere. Consequently, it was assumed that the potassium phase that is precipitated under

reducing conditions must be well dispersed and of a size below the resolution of an optical microscope, i.e., the precipitate must be less than approximately 1 μm. In an attempt to further characterize this second-phase precipitate and also to examine the mode of fracture in these materials, the microstructures were studied using an SEM.

Scanning Electron Microscopy

Samples of each material were fractured at room temperature, mounted on a specimen holder with a conductive silver paste and coated with approximately 40 nm (400 Å) of an evaporated carbon layer prior to examination in an SEM. Particular care was taken so that the reduced materials were exposed to the normal laboratory atmosphere for the minimum of time after fracturing to avoid the formation of any efflorescence. These samples were stored over a silica gel dessicant for 96 hr prior to examination. A comparison of the fracture surface of x = 1.8 material fired under oxidizing and reducing conditions can be made from the SEM micrographs of Figure 41. It can be seen that this material exhibits intragranular fracture whether fired under oxidizing or reducing conditions. In addition, both samples show the presence of both intergranular and intragranular porosity although in the case of the H_2-fired material there is much less of the intragranular porosity in the size range 0.5 μm to 2 μm.

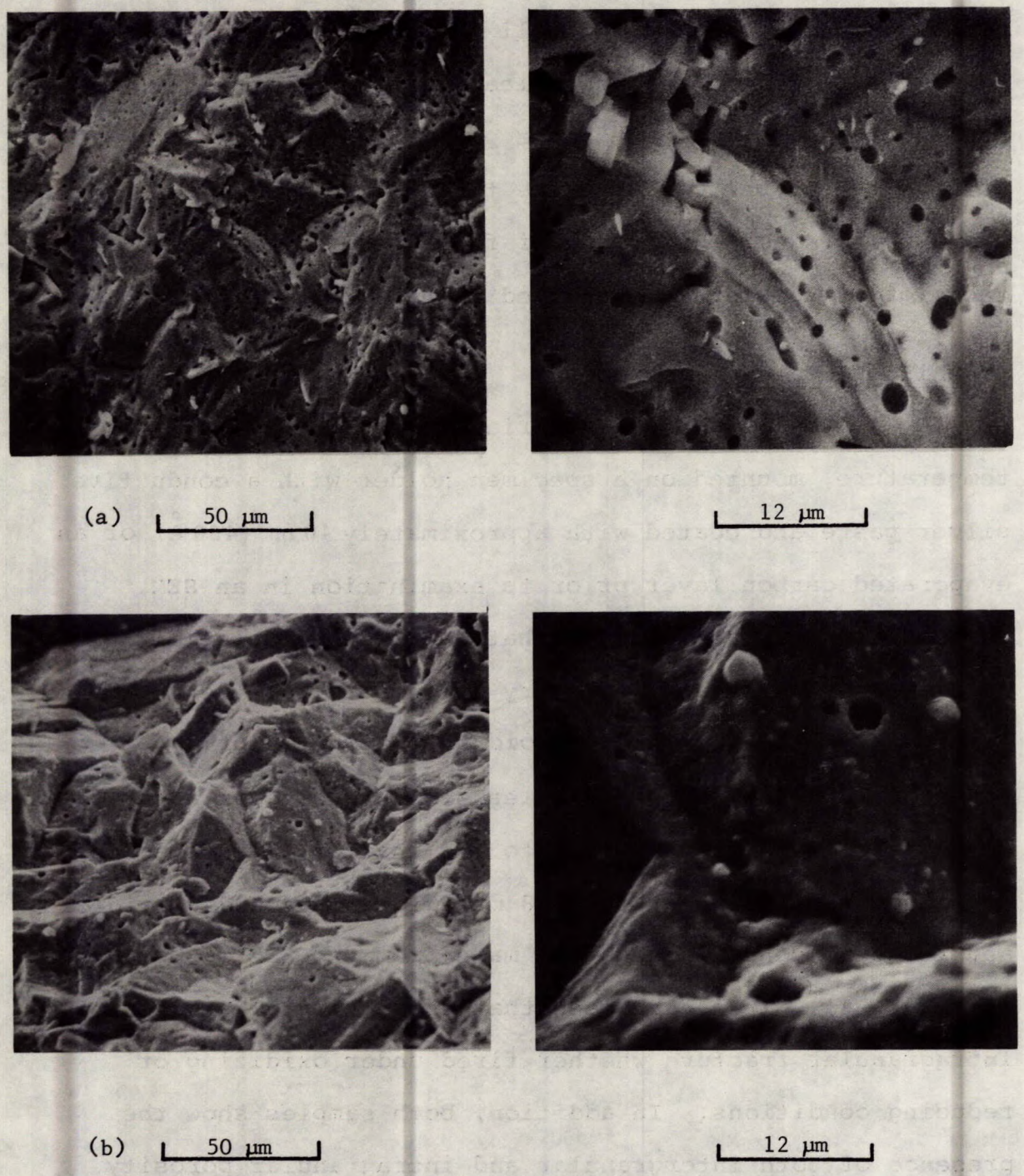

Figure 41. Comparison of the fracture surfaces of x = 1.8 material fired to 1250°C for 3 hr under controlled atmosphere

(a) Oxygen atmosphere
(b) 5% H_2-95% N_2 atmosphere.

At high magnification, a difference between the oxidized and reduced material becomes evident: the oxidized sample exhibits a relatively smooth fracture surface whereas the reduced material shows a surface roughening due to the presence of approximately 0.5-μm projections separated by a mean distance of 2 to 3 μm (the two 4-μm diameter features seen in Figure 41 b are believed to be adventitious material). Unfortunately, it was not possible to confirm that these surface projections are rich in K using the energy dispersive X-ray spectrometer of the SEM as the beam can not be focused finely enough to exite only these specific areas without also including some of the matrix. However, it is most probable that the projections are zones of potassium oxide precipitated throughout the material during firing and which eventually hydrate and pick up CO_2 to form the efflorescence observed on these reduced materials. The general distribution of the K precipitate (rather than being a surface effect alone) was demonstrated by the development of efflorescence on a freshly exposed fracture surface of a sample that had been washed in water and dried prior to breaking: the washed surfaces did not develop as much efflorescence as the newly exposed surfaces.

Subsequently, the fracture surfaces of material fired in oxygen were examined as a function of composition, Figure 42. In each case, the inter and intragranular porosity can be seen. It is interesting to note that the

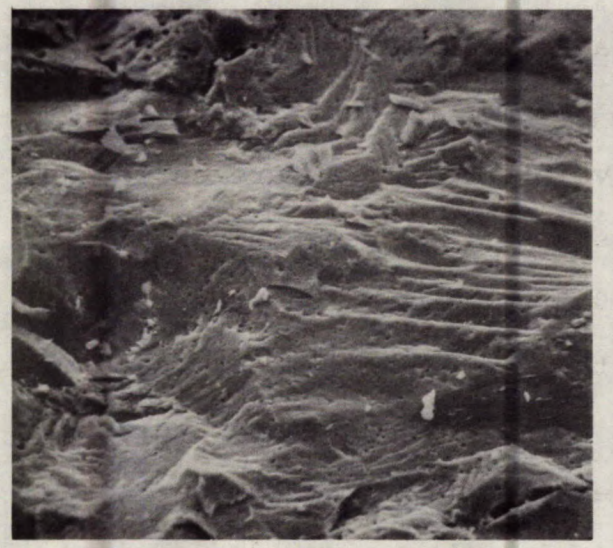

Composition 1.5

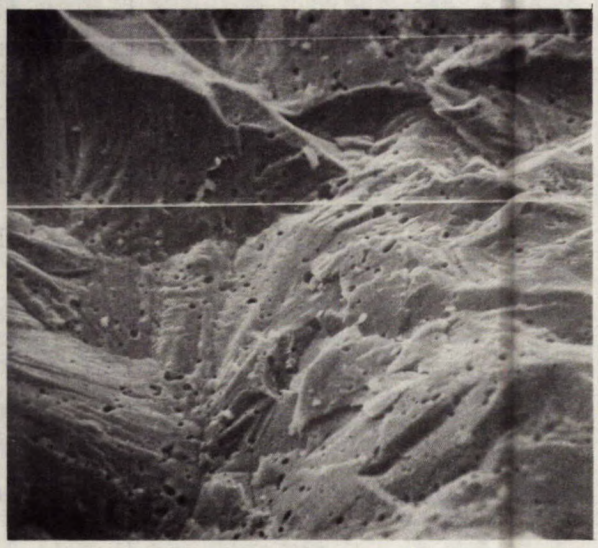

Composition 1.6

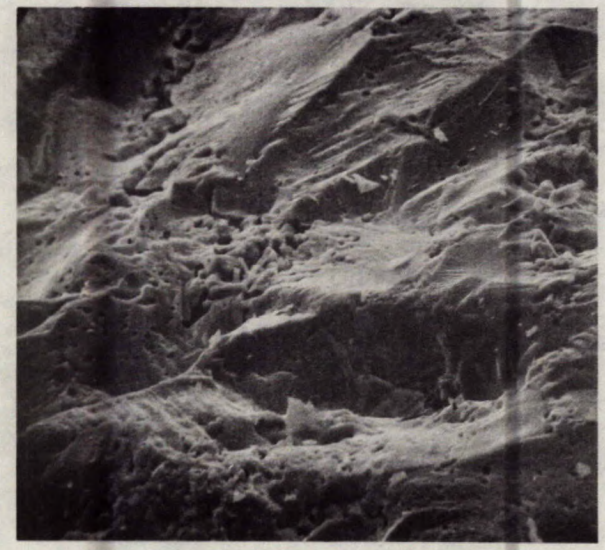

Composition 1.7

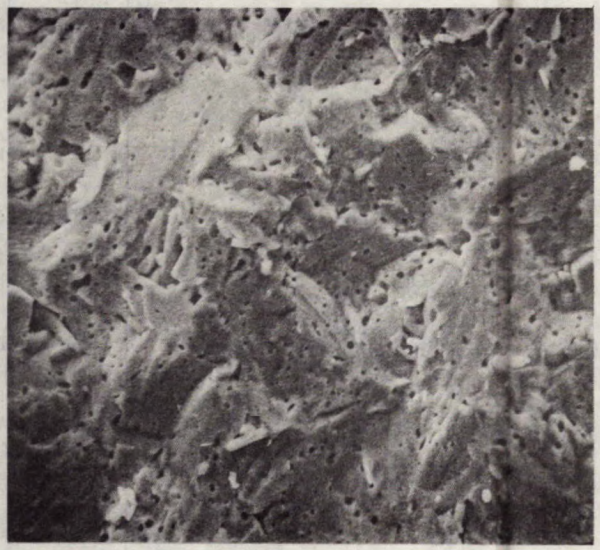

Composition 1.8

50 μm

Figure 42. Comparison of the fracture surfaces of materials fired to 1250°C for 3 hr in an oxidizing atmosphere.

micrograph of the x = 1.7 material shows a bimodal grain size distribution, yet the same material observed under the optical microscope (Figure 34 a) does not. As the size of the smaller grains is well within the resolution of the optical microscope, it is clear that this difference is due to sampling, i.e., the sintering conditions of 1250°C for 3 hrs are only just adequate to allow development of secondary grain growth from a very porous matrix of tabular crystals.

CONCLUSIONS

Highly reactive, homogeneous raw materials having the general formula: $K_xMg_{x/2}Ti_{8-x/2}O_{16}$ can be prepared using a wet chemical procedure in which freshly precipitated $Ti(OH)_4$ is doped with solutions of potassium and magnesium acetates, spray frozen, freeze dried, and finally calcined. Using these materials it has been shown that single-phase sintered material can be produced in the composition range $1.5 \leq x \leq 1.8$; at lower values of x, free rutile (TiO_2) is formed, whereas at higher values a new phase is developed that is isostructural with $K_yLi_yTi_{4-y/2}O_8$, i.e., this phase probably has the composition $K_2MgTi_3O_8$.

Despite the use of a wet-chemical technique to prepare an intimate and homogeneous mixture of the reactants, each composition still follows a complex reaction path during calcination prior to developing single-phase hollandite. For

example, on heating, the compositions x = 1.6, 1.7 and 1.8 follow the reactions:

$$\text{Freeze Dried Material (Amorphous + Trace Anatase)} \xrightarrow{200°C} \text{Anatase} + \text{Trace } (COOK)_2 \xrightarrow{400\text{-}500°C}$$

$$\text{Anatase} + K_2MgTi_3O_8 \xrightarrow{600\text{-}700°C} \text{Rutile} + K_2MgTi_3O_8 + K_xMg_{x/2}Ti_{8-x/2}O_{16}$$

$$\xrightarrow{700\text{-}800°C} \text{Rutile} + K_xMg_{x/2}Ti_{8-x/2}O_{16} \xrightarrow{900°C} K_xMg_{x/2}Ti_{8-x/2}O_{16}$$

However, it has been shown that the wet-chemical process enables homogeneous sintered bodies to be prepared in the composition range $1.5 \leq x \leq 1.8$ whereas only heterogeneous materials can be prepared using a conventional ball-milling technique to mix the reagents.

The density of the sintered products was found to be slightly dependent on the temperature of calcination of the raw material (being higher with a lower temperature calcine) and strongly dependent on the sintering temperature in the temperature range 1150°C to 1250°C. In addition, all compositions suffer an extremely rapid grain growth between 1200°C and 1250°C, in which temperature range the grain size increases nearly two orders of magnitude. Other processing variables such as fabrication pressure, rate of binder burnout, heating rate,and the time at maximum temperature were found to have only a minor influence on the fired density and microstructure.

The single most important parameter in firing these materials was shown to be the furnace atmosphere. All the compositions were found to be sensitive to the oxygen concentration of the atmosphere and also to its water content. The tendency for partially reduced material to be formed on firing in air increased as the concentration of TiO_2 in the body increased, i.e., as x decreased.

A synergistic effect was found between the oxygen concentration and water content of the atmosphere during sintering. For example, although fully oxidized samples could be prepared for all materials in the range $1.5 \leq x \leq 1.8$ using a very high flow rate of nominally dry oxygen gas, only $x = 1.8$ and 1.7 materials remained oxidized in a low flow rate of the same gas. Both the $x = 1.6$ and 1.5 materials were partially reduced and the degree of reduction increased as x decreased. However, by progressively increasing the water content of the gas, these materials could also be oxidized: the greater amount of water being required with lower values of x.

Sintering in hydrogen-containing atmospheres produced completely black material irrespective of composition. These reduced products were found to be unstable in a normal atmosphere and to develop a considerable amount of surface efflorescence due to the hydration and carbonation of a free potassium-rich phase, probably K_2O, which is precipitated throughout the samples in 0.5 -μm zones.

ACKNOWLEDGEMENTS

The authors wish to express their appreciation to all members of the Industrial Minerals Laboratory and of the CANMET staff who contributed to this report.

Thanks are particularly due to A. J. Hanson who conducted much of the technical and processing aspects and to G. Lemieux for thermal analyses and assistance in drafting.

REFERENCES

1. Kiukkola, K. and Wagner, C. "Measurements on galvanic cells involving solid electrolytes"; J. Electrochem. Soc.; v. 104, no. 6, pp 376-387; 1957.

2. Rapp, R.A. and Shores, D.A. "Physicochemical measurements in metals research. Part 2"; Ed. R.A. Rapp; Wiley-Interscience, New York; p 123; 1970.

3. "The DS 2000 electrochemical oxygen monitor"; available from Simac Ltd., Simac House, Lyon Road, Hersham, Walton-on-Thames, Surrey, KT12 3PU, U.K.

4. Wheat, T.A. "Development of a zirconia electrolyte for use in a steel-making oxygen probe"; CANMET Report 76-13; 1976.

4b. Wheat, T.A. "Pilot-plant testing of a zirconia-based oxygen probe"; J. Can. Ceram. Soc.; v. 45, pp 5-13; 1976.

5. Scholes, W.A. "Isa oxy probe advances quality control and automation in copper refining" Eng. and Min. J.; October, pp 82-85; 1974.

6. "Research on electrodes and electrolyte for the Ford sodium-sulphur battery"; Joint research conducted by the Ford Motor Company, Rensselaer Polytechnic and the University of Utah under RANN, Division of Advanced Energy Research and Technology, Washington, D.C. Contract number NSF-C805 (AER-73-07199).

7. "Chloride Silent Power Limited" Davy Road, Astmoor, Runcorn, Cheshire, WA7 1PZ, U.K. This company was created as a joint venture between the Electricity Council and the Chloride Group to develop the sodium-sulphur battery. At that time (1974), parallel R & D programmes were also underway in the British Rail Laboratories, Derby and in the UKAEA Laboratories, Harwell. Subsequently, these laboratories agreed to collaborate on the development of this battery.

8. Worrell, W.L. "Electrochemistry of ceramic electrolytes"; Am. Ceram. Soc. Bull.; v. 53, no. 5, pp 425-433; 1974.

9. DeLong, R.B. "Deoxidation of metal"; News in Engineering; Published by Ohio State University; pp 6-7; May 1972.

10. Arora, A.R. and Childs, J. "Thin film deposition of solid electrolyte $Ag_{19}I_{15}P_2O_7$"; J. Electrochem. Soc.; v. 123 no. 2, pp 222-223; 1976.

11. Unican Electrochemical Products Ltd., 5795 De Gaspe Ave., Montreal, Que.

12. Takahashi, T. and Kuwabara, K. "Preparation of sintered oxides with hollandite-type structure ($K_xMg_{x/2}Ti_{8-x/2}O_{16}$) and their ionic conduction"; Nippon Kagaku Kaishi; v. 10, pp 1883-1887; 1974.

13. Roth, R.S., Parker, H.S., and Brower, W.S. "Crystal chemistry of lithium in octahedrally co-ordinated structures, III A new structure-type in the system K_2O-Li_2O-TiO_2 ($K_xLi_xTi_{4-x/2}O_8$)"; Mat. Res. Bull.; v. 8, pp 323-327; 1973.

14. Wheat, T.A. and Mirkovich, V.V.; Unpublished data; 1970.

15. Wheat, T.A. "Preparation and characterization of lime-stabilized zirconia"; J. Can. Ceram. Soc.: v. 42, pp 11-18; 1973.

16. Mirkovich, V.V. and Wheat, T.A. "Use of liquid nitrogen in spray freezing"; Amer. Ceram. Soc. Bull.; v. 49, No. 8, pp 724-725; 1970.

17. Mirkovich, V.V., Quon, H.H., and Wheat, T.A. "Thermal diffusivity of potassium magnesium titanates having a hollandite structure"; presented at 15th International Thermal Conductivity Conference in Ottawa, August 24-26, 1977.

18. Buist, D.S. "Investigations with the Leitz heating-microscope type IIA-P in the field of ceramics"; Trans. Brit. Ceram. Soc.; v. 69, no. 1, pp 15-20; 1970.

19. MacDonald, W.A., Wheat, T.A., and Quon, H.H. "A method for the rapid mounting and polishing of ceramic materials for microstructural examinations"; CANMET, Laboratory report MRP/MSL 76-276(J); 9 pp; To be published in the J. Mat. Sci.; November 1976.

20. MacKenzie, K.J.D. and Melling, P.J. "The calcination of titania: II The influence of atmosphere on crystal growth in anatase powders"; Trans. and J. Brit. Ceram. Soc.; v. 73, no. 6, pp 179-183; 1974.

APPENDIX A

DETERMINATION OF THE QUANTITY OF POTASSIUM AND MAGNESIUM ACETATE REQUIRED TO PRODUCE A SPECIFIC CONCENTRATION OF POTASH AND MAGNESIA IN TITANIA

Concentration of Titania Slurry

Samples of the slurry were taken from the main batch after washing to remove Cl^- contamination. After stirring vigorously for 2 hr, the precipitate was divided into essentially equal parts by transferring into weighed containers. At this point, samples of slurry were taken to determine concentration. In each case, duplicate 25-mL aliquots were withdrawn and placed in weighed Pt dishes that were subsequently dried at 110°C overnight and then ignited to constant weight at 1000°C.

		Sample (i)	Sample (ii)
Wt of slurry (g)	=	25.1545	25.2302
Wt TiO_2 formed (g)	=	0.8469	0.8455
Concentration of slurry (g TiO_2/g slurry)	=	0.03367	0.03351
Average conc of slurry (g TiO_2/g slurry)	=	0.03359	

Loss on Ignition of Potassium and Magnesium Acetates

Unfortunately, it was not possible to accurately determine the ignition loss of $CH_3.COOK$ because this material

melts at 294°C and tends to eject material from a crucible prior to decomposition. Consequently, the ignition loss of this material was assumed to be that given by stoichiometry, i.e., 1 mol of K_2O is formed from 2 mol of acetate.

The weight loss of the $(CH_3.COO)_2Mg$ component was found to be 80.91% on ignition to 1000°C for 1 hr. This value is slightly below the theoretical loss of 81.4% for pure $(CH_3.COO)_2$ Mg. $4H_2O$.

Quantity of Each Acetate Required to Dope Slurry

From the weight of each batch and the slurry concentration, the quantity of TiO_2 in each separate batch was determined. The example given below illustrates the formulation of a doped titanate having the composition: $0.8K_2O:0.8MgO:7.2TiO_2$, i.e., where x equals 1.6.

Mass TiO_2 g	Mol TiO_2	Need Mol K_2O	Need Mol MgO	Need Mol K.Ac*	Need Mol $Mg.Ac_2$	Wt K.Ac Needed g	Wt $Mg.Ac_2$ Needed g**
39.6022	0.4956	0.0550	0.0550	0.1101	0.0550	10.8081	11.7953

*Ac: acetate group, i.e., $CH_3.COO-$

**Because of the slight difference between the theoretical weight loss and that determined in practice, the quantity of $Mg.Ac_2$ shown above was increased by a factor 81.4/80.9 to 11.8682 g.

These quantities of each acetate were dissolved in distilled water to give two separate 0.5-molar solutions that were subsequently mixed together and added slowly to the vortex of the vigorously stirred slurry.

APPENDIX B

FURNACE ATMOSPHERIC CONDITIONS REQUIRED TO PRODUCE A FULLY OXIDIZED SINTERED PRODUCT

Composition, x	Gas Flux and Composition*
1.8	6 $g/cm^2/hr$ of dry oxygen
1.7	6 $g/cm^2/hr$ of dry oxygen
1.6	6 $g/cm^2/hr$ of wet oxygen containing 1.78 wt % water vapour** OR 20 $g/cm^2/hr$ dry oxygen+
1.5	6 $g/cm^2/hr$ of very wet oxygen containing 45.66 wt % water vapour*** OR 20 $g/cm^2/hr$ dry oxygen+

*In the present work, a gas flow rate of 85 L/hr or 285 L/hr was introduced into a 5-cm diameter horizontal tube furnace to give a gas flux of either 6 $g/cm^2/hr$ or 20 $g/cm^2/hr$.

**A concentration of 1.78 wt % water vapour in the oxygen gas stream was obtained by passing the gas at 85 L/hr through water at 24°C prior to introducing into the furnace.

***A concentration of 45.66 wt % water vapour was obtained by passing the oxygen at 85 L/hr through water at 93°C prior to introducing into the furnace.

+Although a flux rate of 20 $g/cm^2/hr$ of dry oxygen produces fully oxidized material, it requires a gas velocity of ∿17 m/sec in the 6-mm diameter inlet tube to the furnace. This high velocity gas stream impinges directly on the sample during sintering and leads to a considerable cooling effect and the development of badly cracked and warped discs. It is for this reason that the lower flux rate of oxygen of 6 $g/cm^2/hr$ containing 45 wt % of water vapour was used.

The above conditions apply to temperatures above 700°C during both the heating and cooling cycle of the sintering stage.

CANMET REPORTS

Recent CANMET reports presently available or soon to be released through Printing and Publishing Supply and Services, Canada (addresses on inside front cover), or from CANMET Publications Office, 555 Booth Street, Ottawa, Ontario K1A 0G1:

Les récents rapports de CANMET, qui sont présentement disponibles ou qui ce seront bientôt peuvent être obtenus de la direction de l'Imprimerie et de l'Edition, Approvisionnements et Services, Canada (adresses au verso de la page couverture), ou du Bureau de Vente et distribution de CANMET, 555 rue Booth, Ottawa, Ontario, K1A 0G1:

77-14 Pit slope manual - Chapter 7 - Perimeter blasting; P. Calder;
Cat. No. M38-14/7-1977, ISBN 0-660-01011-9; Price: $2.25 Canada, $2.70 other countries.

77-16 Pit slope manual - Supplement 5-1 - Plane shear analysis; D.F. Coates;
Cat. No. M38-14/5-1977-1, ISBN 0-660-01008-9; Price: $4.25 Canada, $5.10 other countries.

77-19 Pit slope manual - Supplement 2-2 - Domain analysis programs; D. Cruden and J. Ramsden;
Cat. No. M38-14/2-1977-2, ISBN 0-660-00990-0; Price: $3.75 Canada, $4.50 other countries.

77-23 Pit slope manual - Supplement 2-4 - Joint mapping by terrestrial photogrammetry; G. Herget;
Cat. No. M38-14/2-1977-4, ISBN 0-660-00992-7; Price: $2.50 Canada, $3.00 other countries.

77-24 Pit slope manual - Supplement 2-5 - Structural geology case history; G. Herget;
Cat. No. M38-14/2-1977-5, ISBN 0-660-00993-5; Price: $2.75 Canada, $3.30 other countries.

77-30 Pit slope manual - Supplement 4-1 - Computer manual for seepage analysis; J. Marlon-Lambert;
Cat. No. M38-14/4-1977-1, ISBN 0-660-01007-0; Price: $3.50 Canada, $4.20 other countries.

77-31 Pit slope manual - Supplement 10-1 - Reclamation by vegetation - Vol. 1 - Mine waste description and case histories; D. Murray;
Cat. No. M38-14/10-1977-1, ISBN 0-660-01013-5; Price: $3.50 Canada, $4.20 other countries.

77-47 Statistical correlation of ASTM and JIS coke tumbler test results; W.R. Leeder and K.A. Jonasson;
Cat. No. M38-13/77-47, ISBN 0-660-01705-9; Price: $1.25 Canada, $1.50 other countries.

77-56 Corrosion protection and lateral displacement characteristics of rock anchors; R. Sage;
Cat. No. M38-13/77-56, ISBN 0-660-01806-3; Price: $1.25 Canada, $1.50 other countries.

77-58 Pit slope manual - Supplement 10-1 - Reclamation by vegetation - Vol. 2 - Mine waste inventory by satellite imagery; D. Murray;
Cat. No. M38-14/10-1977-1-2, ISBN 0-660-01464-5; Price: $6.00 Canada, $7.20 other countries.

77-60 The high-temperature behaviour of blast furnace coke - A review; D.A. Reeve, J.T. Price and J.F. Gransden;
Cat. No. M38-13/77-60, ISBN 0-660-01807-1; Price: $1.25 Canada, $1.50 other countries.

77-61 A rapid method for the determination of sulphur and vanadium in petroleum products by non-dispersive x-ray fluorescence; R. Makhija, R.G. Draper and E. Furmisky;
Cat. No. M38-13/77-61, ISBN 0-660-01848-9; Price: $1.00 Canada, $1.20 other countries.

77-65 Performance of superplasticizers in concrete: Laboratory investigation - Part 1;
V.M. Malhotra and D. Malanka;
Cat. No. M38-13/77-65, ISBN 0-660-01739-3; Price: $1.75 Canada, $2.10 other countries.

78-2 Revision of recommended values for reference ores MP-1 and KC-1; G.H. Faye and W.S. Bowman;
Cat. No. M38-13/78-2, ISBN 0-660-01712-1; Price: $1.00 Canada, $1.20 other countries.

78-3 Certified and provisional reference materials available from the Canada Centre for Mineral and Energy Technology, 1978; G. Faye;
Cat. No. M38-13/78-3, ISBN 0-660-01804-7; Price: $1.25 Canada, $1.50 other countries.

76-40F Evaluation des charbons marchands canadiens: Nouvelle-Ecosse et Nouveau Brunswick - 1975;
T.E. Tibbetts et W.J. Montgomery;
Cat. No. M38-13/76-40F, ISBN 0-660-01821-7; Price: $3.00 Canada, $3.60 other countries.